Insights into formation and properties of amorphous mesostructured alumina

Jean-Luc Blin, Florian Jonas, Laure Michelin, Séverinne Rigolet, Ludovic Josien, Loïc Vidal, Lionel Richaudeau, Bénédicte Lebeau

Insights into formation and properties of amorphous mesostructured alumina

Jean-Luc Blin[1*], Florian Jonas[1], Laure Michelin[2,3], Séverinne Rigolet[2,3], Ludovic Josien[2,3], Loïc Vidal[2,3], Lionel Richaudeau[1], Bénédicte Lebeau[2,3*]

[1]: Université de Lorraine, CNRS, L2CM, F-54000 Nancy, France
[2] : Université de Haute Alsace (UHA), CNRS, IS2M UMR 7361, F-68100 Mulhouse, France
[3] : Université de Strasbourg, F-67000 Strasbourg, France

* Corresponding authors : Jean-Luc.Blin@univ-lorraine.fr, Benedicte.Lebeau@uha.fr

Abstract
Here, using liquid crystals as template, an EISA (evaporation-induced self-assembly) method has been used to synthesize amorphous mesostructured alumina. The effect of the synthesis parameters such as the presence of a chelating agent, the amounts of both porogen agent and alumina precursor on the materials properties have been investigated in details. Under the optimum conditions, after Soxhlet extraction, the obtained Al_2O_3 presents an HMS (Hexagonal Molecular Sieves) structure and a high specific surface area (≈ 400m²/g) with a mesopore size distribution centered around 8.3 nm.
Investigation of the thermal stability shows that the crystallization into γ-Al_2O_3 of the amorphous alumina walls delimiting mesopores begins after heating at 800°C. We have also demonstrated that half of the carbon present in the as-synthesized material can be removed by washing with water or ethanol at room temperature instead of Soxhlet extraction.
On the basis of SAXS, XRD and N_2 adsorption-desorption analyses, we have shown that when treated into boiling water or exposed to water vapor the alteration of the mesostructure occurs quickly. Its collapse has been attributed to the crystallization of the amorphous alumina walls into aluminum hydroxides, mainly boehmite, upon the hydration of the alumina.
Dual mesoporous alumina have been also obtained from micelles through a cooperative templating mechanism at low P123 amount and in the presence of citric acid. In that case both mesopores networks adopt a wormhole-like mesostructure.

Keywords : Mesostructured Alumina; Soft Templating; Dual Mesoporosity; Thermal Stability; Hydrothermal Stability

1. Introduction

Thanks to its properties in particular the acidic ones [1,2], alumina catalyzes a variety of reactions that are useful industrially [3,4]. For example, in its largest scale of applications, alumina is the catalyst in the Claus process for converting hydrogen sulfide waste gases into elemental sulfur in refineries [5,6], it is used for dehydration of alcohols to alkenes [6-9] and so on [6]…. Alumina also serves as a catalyst support for many industrial catalysts due to its ability to disperse the supported active phase, its high thermal stability as well as for its moderate price [6]. The good dispersion of the active phase is associated with the presence of acid/base sites on its surface (hydroxyls). For instance, it is used as support in petroleum industry for hydrotreating [4,10]. Moreover, alumina is usually prepared as fine divided powder with large surface area and thus with a large number of accessible active sites. So, it is more effective to use a finely divided form of catalyst in reaction. The most common crystalline phase of alumina is α-Al_2O_3 known as corundum , which is the thermodynamically stable form [11]. The oxygen ions form a nearly hexagonal close-packed structure with the aluminum ions filling two-thirds of the octahedral interstices. Each Al^{3+} center is octahedral. In terms of crystallography, corundum adopts a trigonal Bravais lattice with a space group of R-$\bar{3}$c (number 167 in the International Tables). The primitive cell contains two formula units of alumina [11]. Alumina also exists in other metastable phases, including the cubic γ and η ones, the monoclinic θ, the hexagonal χ, the orthorhombic κ and the δ phases [6,11]. The latter one can be tetragonal or orthorhombic. Each phase has a unique crystal structure and properties. Among alumina crystalline phases γ-Al_2O_3 is the most used form for catalysis applications [12-15]. To develop the applications of alumina in catalysis, adsorption and so on, recently must efforts have been devoted to reduce the synthesis costs, to improve its properties and to simplify the synthesis procedures. Especially, increasing the specific surface area of alumina could potentially enhance the catalytic activity [16,17]. One way to increase the specific surface and reduce the costs consist in preparing mesoporous aluminosilicate [18-20] instead of pure alumina. In that case the use of composite template can contribute to reduce the synthesis cost. Another approach to increase the alumina specific surface area deals with the preparation of mesostructured Al_2O_3. Different strategies including, nano-casting, the sol-gel process associated with surfactant based-systems, the Evaporation Induced Self Assembly (EISA) or the mechanochemical solid-state route, have been developed to prepare mesoporous alumina (MA) or organized mesoporous alumina (OMA) [17, 21-41]. In the case of the nano-casting Al_2O_3 is the replica of a mold such as ordered mesoporous silica as hard template. But this procedure is time consuming, non-eco-friendly (it usually requires hydrofluoric acid to remove the hard template) and it is quite difficult to completely fulfill the mesopores of the hard template with the alumina precursor. The soft templating route, which is based on the co-assembly of the alumina precursor and surfactant, as made for the synthesis of ordered mesoporous silica has also some drawbacks. First, the polymerization of the precursors is often incomplete. Second, the release of the porous network often goes through a calcination step, which can lead to the collapse of the mesostructure due to the crystallization of the walls. Finally, another difficulty is associated with the control of the reactivity of the inorganic precursor. Among the surfactant-based methods, the EISA method to get OMA through a one-step approach is an efficiency tool. In that case organic solvents, mainly ethanol, act as reaction medium in presence of block copolymers used as templates, aluminum precursor and acid solution. Using this approach in 2008, Yuan et al. have reported the synthesis of ordered mesoporous γ-Al_2O_3 with specific surface area of 400 m^2/g and high thermal stability [33]. Since this that a series of OMA have been prepared through EISA approach by different groups [35]. However, the EISA pathway requires strict control of the synthesis conditions such as the amount of water, the type of template and solvent, or solution acidity and it usually leads to OMA having high surface area but crystalline pore walls with large pore widths [35]. By

contrast, the mechanochemical synthesis of alumina does not required solvent and the method has been extended to the design of metal aluminate but pollution of the materials by the milling balls can occur. In that case a purification step is needed.
Combining the EISA method and the liquid crystal templating pathway, in our group we have developed a synthesis procedure that allows to obtain amorphous mesostructured titania [42] and zirconia [43] with high specific surface area, high thermal and hydrothermal stability. The mesostructured TiO_2 having a part of amorphous phase were used as supports for the preparation of CoMoS (Co-promoted MoS2) hydrotreatment catalysts [44,45]. The catalysts were tested in the conversion of 46DMDBT. Obtained results, stand out from what has been reported in the past. Firstly, mesostructured titania present a high concentration of Brønsted acid sites on the surface. Secondly, a shift towards DDS selectivity in the conversion of 46DMDBT, which is unprecedented in literature, was observed. The amorphous phase involves modifications in the properties of the oxide support material leading to significant changes in the catalytic properties (HYD/DDS selectivity ratio), which offers unexplored opportunities in catalyst development. Since alumina is one of the most important supports and catalysts, the synthesis of mesostructured alumina having amorphous walls with high thermal and hydrothermal stability is therefore still worth of investigation. Indeed, the presence of amorphous phase will affect the features of the active phase (size, morphology…) and the designed catalysts will have significantly modified activity and selectivity than the corresponding crystalline ones. Here, an extended investigation of our strategy for the synthesis of pure amorphous mesostructured alumina is reported in detail. Our aim is to explore in a rational way the relationships among the inorganic material preparation, and its stability.

2. Experimental

The amphiphilic triblock copolymer Pluronic P123 $(EO)_{20}(PO)_{70}(EO)_{20}$ (EO = ethylene oxide, PO = propylene oxide) purchased from Aldrich was used as the porogen agent. Aluminum tri sec butoxide (Aldrich, 97%) was used as the inorganic precursor. Hydrochloric acid (ACS reagent, 37%, Aldrich), ethanol (99%, Aldrich) and citric Acid (Acros, 99%) were used to control the reactivity of the alumina precursor. Aqueous ammonia (28 wt.%) was purchased from Aldrich.

2.1. Materials preparation: In a typical synthesis: 3 g of surfactant were dissolved under stirring at room temperature in 20 g of ethanol in the presence of 0.5 g of citric acid. Then 1.5 g of a hydrochloric acid solution and 4 g of aluminum tri sec butoxide were added. After stirring during 3 hours, 2 g of water were incorporated. The solvent of the mixture was then directly evaporated under vacuum. Recovered solids were dried in an oven at 40°C during 12 h. Then they were placed under an atmosphere of NH_3 (≈ 0.5 atm) for 12 h. For that step, samples were placed during 12 hours in a well-closed glass vessel containing concentrated aqueous ammonia (28 wt.%) in a crystallizer without touching the sample to saturate the atmosphere in gaseous NH3. The mesostructured alumina was obtained after Soxhlet extraction of the porogen agent using ethanol as solvent during 16 hours. Recovered solids are dried in an oven at 40°C during 12 h.

2.2. Extraction by water or ethanol at room temperature: 0.5 g of the hybrid mesophase was introduced into a 100 mL flask in the presence of 20 g of distilled water or ethanol under stirring. After extraction times, varying from 1 to 48 h, samples were withdrawn by filtration from the solution. They were rinsed three times with 10 mL of distilled water or ethanol and dried in air at 40°C for 24 h in an oven.

2.3. *Thermal stability*: Mesostructured alumina, obtained after Soxhlet extraction and drying in air for 24 hours at ambient temperature, were heated in a muffle furnace under air. The samples were heated to 150°C, at a rate of 1 °C / min and kept at this temperature during one hour. Afterwards, the same program was applied to reach the final temperature, which was varied between 500 and 1100°C. They were kept at the final temperature during 2 hours and cooled down.

2.4. *Hydrothermal stability: In boiling water*: 1.5 g of mesostructured Al_2O_3, previously calcined at 500, 700 or 900°C were placed under reflux at 120 °C in 200 mL of distilled water. The mixture was stirred continuously for 24 hours. Aliquots were taken at regular time intervals, between 30 minutes and 1 day. They were recovered by filtration and dried in air at 40°C for 24 h in an oven.

Exposure to water vapor: In order to investigate the hydrothermal stability of materials in the presence of water vapor, a glass support, composed of two parts, was home made (Scheme 1). 50 mg of material were deposited in the upper part of the support and the lower part was filled with 3 g of distilled water. The support was then transferred into a Teflon autoclave, which was heated at 200°C for 24 hours in an oven. Then, the material was dried for 24 h at 40°C in oven.

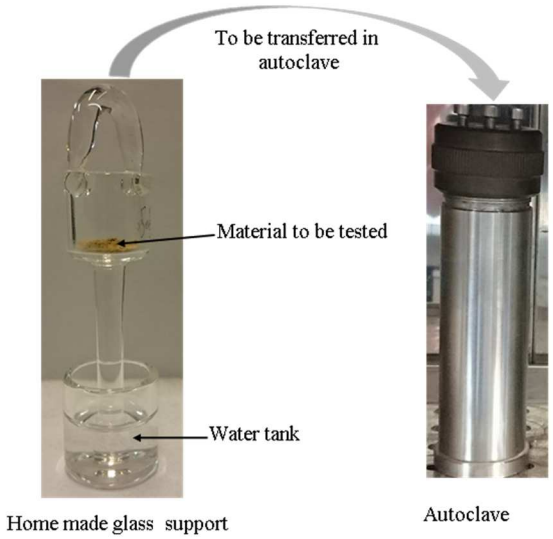

Scheme 1: Scheme of the home made glass support used for the investigation of the hydrothermal stability in the presence of water vapor.

2.5. Characterization: SAXS experiments were performed on a SAXSess mc² instrument (Anton Paar), using a line collimation system. This instrument is attached to a ID 3003 laboratory X-Ray generator (General Electric) equipped with a sealed X-Ray tube (PANalytical, $\lambda_{Cu,\,K\alpha} = 0.1542$ nm) operating at 40 kV and 50 mA. A multilayer mirror and a block collimator provide a monochromatic primary beam. A translucent beam stop allows the measurement of an attenuated primary beam at q=0. Materials were put between two sheets of Kapton® placed in a powder cell before being introduced inside the evacuated chamber. All data were corrected for the background scattering from the Kapton® and for slit-smearing effects by a desmearing procedure from SAXSQuant software using the Lake method. Powder X-ray diffraction patterns were recorded using a PANalytical X'Pert PRO diffractometer equipped with a Cu X-ray tube ($\lambda_{Cu(K\alpha)} = 0.1542$ nm) operating at 45 kV and 40 mA and a X'Celerator detector. Fixed divergence slit (1/16°), mask (10 mm) and antiscatter slit (1/8°) were used at primary beam for the current analysis.

N_2 adsorption-desorption isotherms were determined on a Micromeritics TRISTAR 3000 sorptometer at –196 °C. Prior analyses, samples were outgassed at 25°C under vacuum (0.13 bar) for 16 hours. The specific surface area was obtained by using the BET model whereas the pore diameter and the pore size distribution were determined by the BJH (Barret, Joyner, Halenda) method applied to the adsorption branch [46].
^{27}Al MAS NMR spectra have been recorded at room temperature on a Bruker AVANCE NEO 400WB spectrometer (B_0=9,4T) operating at 104.23 MHz. Samples were packed in a 2.5 mm diameter cylindrical zirconia rotor fitted with Vespel end caps and spun at a spinning frequency of 25 kHz. ^{27}Al MAS NMR experiments were collected with a π/12-pulse duration of 0.33 µs and a recycle delay of 1 s. The number of accumulations varied from 50000 to 90000. The chemical shifts were referenced to external $[Al(H_2O)_6]^{3+}$ in $AlCl_3$ aqueous solution.
Infrared analyzes have been carried out with a Bruker Equinox IFS 55 spectrophotometer equipped with a DTGS detector. Materials (1 mg) were dispersed in a KBr matrix (100 mg) used as a reference before being compacted under 3.5 tons for 2 min in a pelletizer of 13 mm in diameter. The pellets were analyzed with a resolution of 4 cm^{-1} and an accumulation of 32 scans.
Scanning Electron microscopy (SEM) images were recorded with a JEOL JSM-7900F scanning electron microscope (SEM) equipped with a BRUKER QUANTAX spectrometer for the energy dispersive X-ray analyses (EDX).

3. Results

3.1. Effect of the synthesis parameters on the mesostructured alumina formation

Following the EISA strategy, the synthesis of mesostructured alumina was investigated by using aluminum tri sec butoxide as alumina precursor and P123 triblock copolymer as porogen agent. The role played by the citric acid as well as the effect of the amount of both the alumina precursor and the surfactant were investigated. Samples have been characterized after Soxhlet extraction using ethanol as solvent during 16 hours. To start the total mass of acid has been fixed to 2g. When both hydrochloric acid and citric acid are used, their quantity has been chosen to be 1.5 and 0.5g, respectively.
From Figure S1, which depicts the SAXS pattern of the extracted materials prepared in the presence or not of citric acid and by varying the amount of P123 and alumina precursor, it can be observed that no reflection line is detected for samples obtained by using 1 or 2 g of aluminum tri sec butoxide. This means that for these amounts whatever the other parameters, no mesostructure is formed.
In the presence of citric acid, the nitrogen adsorption-desorption isotherms (not shown) are flat when the amount of alumina precursor is equal to 1g. Increasing the latter quantity to 2g, the isotherms are rather type II (Fig. S2). The adsorbed N_2 volumes are low and they decrease with the amount of porogen agent. When detected, the pore size distributions are very broad with very low dV/dD values (insert of Fig. S2). Under these conditions, the obtained materials are almost non-porous. When the syntheses are performed with 1g of P123 and 3-5g of alumina precursor, two inflection points at relative pressure p/p_0 around 0.50-0.6 and 0.75-0.80 are observed on the adsorption branch of the isotherm (Fig. S2A), suggesting that two pore systems with different diameters arranged in a three-dimensional pore structure are present. In these latter cases, the hysteresis at the desorption is type H2(a) indicating either to pore-blocking/percolation in a narrow range of pore necks or to cavitation-induced evaporation [46]. Two components at 5.5 and 11. 2 nm for the materials prepared using 3 g of precursor are observed on the pore size distribution (Table 1, insert of Fig. S2A). For this sample, the coexistence of the two mesopores networks is further confirmed by the SAXS analysis, indeed two reflections lines at 19.7 and 9.3 nm are observed on the SAXS pattern (Fig. S1B). Increasing the aluminum tri sec butoxide quantity the second capillary condensation (p/p_0 =

0.75) is less pronounced and it completely disappears for 6g of precursor. Looking at the pore size distribution (insert of Fig. S2A), the component at 5.5 nm is shifted towards lower values, while the second one progressively disappears and for 6g of precursor the material has a monomodal pore size distribution centered at around 4.2 nm. Meantime, a weak intense and broad reflection line at 13.1 nm is observed on the SAXS pattern (Fig. S1B). The dual mesoporosity is also detected for the sample prepared with 2g of P123 and 4g of aluminum tri sec butoxide (Fig. S1B and S2B). All other materials prepared in the presence of citric acid have a monomodal pore size distribution (insert of Fig. S2B and Fig. S2C). Type IV isotherms with high and steep condensation step and H_1 hysteresis that characterize cylindrical mesopores were obtained for these materials. Their SAXS pattern mainly exhibit only one broad reflection characteristic of wormhole-like mesostructured [47,48]. It should be noted that on the SAXS pattern of the alumina synthesized using 3g of porogen agent and 4g of aluminum tri sec butoxide two diffraction peaks at 10.3 and 5.2 nm are clearly visible (Fig. S1B). The second peak is a harmonic of the first one and their presence characterize the formation of an HMS (Hexagonal Molecular Sieves) mesostructure of cylindrical mesopores [49]. As reported by Pinnavaia et al. for this kind of mesostructure higher order Bragg reflections are not resolved in the patterns [50]. They exhibit mainly a single reflection accompanied by more or less pronounced diffuse scattering at higher q values.

Table 1: Variation of the specific surface area (S_{BET}), of the pore volume (Vp) and of the mesopore diameter (∅) as a function of both the amount of P123 and aluminum tri sec butoxide. Materials have been prepared without addition or in the presence of citric acid.

P123 (g)	Al tri-sec butoxide (g)	Ethanol + HCl			Ethanol + HCl + citric acid		
		S_{BET} (m^2/g)	V_P (cm^3/g)	∅ (nm)	S_{BET} (m^2/g)	V_P (cm^3/g)	∅ (nm)
1	1	47	0.06	6.5	-	-	-
	2	67	0.08	5.1	47	0.13	10.3
	3	307	0.60	10.1	275	0.42	5.5/11.2
	4	235	0.59	12.3	259	0.37	5.1/12.7
	5	182	0.61	17.9	210	0.28	4.5/12.0
	6	211	0.49	11.1	203	0.25	4.2
2	1	92	0.13	4.7	-	-	-
	2	256	0.21	3.7	12	0.03	10.3
	3	246	0.29	5.1	203	0.39	8.2
	4	284	0.44	5.4	387	0.81	7.5/14.1
	5	315	0.94	13.0	383	0.72	6.9
	6	318	0.73	9.0	345	0.61	6.4
3	1	88	0.11	5.8	-	-	-
	2	76	0.25	7.5	2	-	-
	3	62	0.11	6.5	45	0.07	8.4
	4	176	0.23	5.1	403	0.83	8.3
	5	318	0.73	6.4	387	0.71	7.5
	6	379	1.27	12.4	351	0.59	6.5

- Almost non porous materials

For materials prepared without the addition of citric acid, no dual mesoporosity is detected by nitrogen adsorption-desorption analysis (Fig. S3). Except for materials synthesized with 2g of P123 and 5 or 6g of aluminum tri sec butoxide, the capillary condensation is spread out a wide range of relative pressure. The dV/dD values are lower than the ones obtained in the presence of citric acid. The isotherms are of type IV, but the pore size distributions are broader (insert of

Fig. S3) than those obtained in the presence of citric acid (insert of Fig. S2). SAXS patterns depicted in Figure S1B present either no reflection peak or broad and not well-defined reflection lines. Moreover, from Figure S1 it can be also deduced that in a general way, the presence of the citric acid, which acts as a chelating agent, has a beneficial effect on the mesostructuration. For example, while no reflection line is observed on the SAXS pattern of the alumina synthesized using 2g of P123 and 3g of aluminum tri sec butoxide (Fig. S1A), a peak at 12.4 nm is observed when citric acid is added (Fig. S1B).

Overall, considering the error on measurement, for a given quantity of P123, the specific surface area increases or remains constant with the quantity of aluminum tri sec butoxide (Table 1).

The synthesis strategy is based on a combined LCT/EISA (LCT for Liquid Crystal Templating) route that has been successfully developed to produce mesostructured titania and zirconia [42,43]. The porogen agent is first dissolved in a large amount of ethanol then the alumina precursor is added. The large amount of ethanol prevents the formation of a gel and in order to control the reactivity of the inorganic precursor, materials have been prepared in the presence of hydrochloric acid. After addition of water the solvent is quickly extracted with rotating evaporator at 55°C. Regarding the amounts of P123, HCl solution and water, the materials have been prepared with a P123 concentration in the acidic solution of 22, 36 and 46 wt.%. Referring to the P123/water phase diagrams [51,52] the first value is located in the micellar domain (L_1), the second and the third belong to the I_1 and H_1 phase, respectively. It should be noted that the limits of the liquid crystals' domains of P123 in water are not modified in a hydrochloric acid solution [42].

Considering materials prepared with 2 or 3 g of P123, during the evaporation step the liquid crystal is formed and it serves as a mold and with which the inorganic precursor interacts through electrostatic and/or van der Waals forces. The mesostructuration will be also affected by the rates of hydrolysis and condensation of the inorganic precursor, which can be slowed down by performing the synthesis under strong acidic conditions and possibly using a chelating agent. However, because of its volatility [38], a part of HCl is likely removed with the solvent during the evaporation step. This reduces the acidity of the medium and makes hydrolysis and condensation faster. Moreover, chloride ions can strongly coordinate with aluminum ones, preventing the interaction of aluminum species with the porogen agent. The combination of these two effects can explain why no mesostructuration is observed for materials prepared with 1g and 2g of inorganic precursor.

If the quantity of aluminum tri sec butoxide is raised, since the amount of HCl remains constant, more aluminum species are available to interact with the porogen agent and the inorganic-organic interface is less affected by the presence of Cl^-. As a consequence, the formation of the hybrid mesostructure is less disturbed and wormhole like mesostructured alumina are recovered. One way to counteract the negative effect of the Cl^- ions on the mesostructuration is to introduce citric acid as a chelating agent [33,38]. The interactions between the citrate and aluminum ions will slow down the reactivity of aluminum species and then promote the formation of the hybrid mesophase. Another beneficial effect of the presence of the citric acid is that it will not be eliminated during the evaporation step since it is non-volatile [33,38]. As a result, it will contribute to maintain the acidity of the medium and therefore to better control the condensation of the inorganic precursor. Nevertheless, here even in the presence of citric acid at the best we obtain a HMS type structure. A possible reason may be the presence of water, which promotes the hydrolysis of the aluminum precursor and thus affects the homogeneity of the particles [53]. Indeed, in a paper dealing with the role of the solvent in the preparation of mesoporous alumina using aluminum isopropoxide, Wu et al. have reported that the use of an ethanol/water mixture instead of pure ethanol leads to the formation of less homogeneous particles with wormhole morphologies. An enlargement of the pore size distribution and a decrease of the specific surface area are also noted. The authors have

attributed this phenomenon to the faster hydrolysis of aluminum precursor due to the presence of water [53].
When materials are prepared with 1g of P123, i.e. 22% of P123 in the acidic solution, the situation is quite different since alumina are obtained from micelles and not from liquid crystals. In that case, the cooperative mechanism rather predominates. In the absence of citric acid, as observed for materials synthesized from I_1 and H_1, the interactions between the hydrolyzed precursor and the porogen agent are disturbed because of the reduction of the solution acidity caused by the partial evaporation of the hydrochloric acid but also by the coordination of Cl^- with aluminum ions. As a result, monomodal wormhole-like mesostructure with rather broad mesopore size distribution are obtained. In the presence of citric acid, we have also to consider the interaction of citrate ions with the porogen agent. Looking at the position of citrate ion in the Hofmeister series [54], this ion is known to have a salting out effect and the interactions between P123 and citrates ions involve a shift of the lower consolute boundary toward lower temperatures, i.e. the demixion temperature is decreases. It can thus be inferred that the evaporation at 55°C leads to a biphasic system and the alumina source polymerizes around surfactant aggregates, which have different sizes, as observed in the case of bimodal mesostructured silica prepared from micellar solution of fluorinated surfactants [55]. This leads to the formation of the dual mesostructured alumina. Increasing the aluminum precursor amount, more and more citrate ions are coordinated with aluminum ones and therefore there are fewer and fewer citrate ions available to interact with P123. The salting out effect diminishes and it completely disappeared when 6g of aluminum tri sec butoxide are used during the synthesis. Consequently, the second component in the mesopore distribution progressively disappears and the system becomes monomodal. Considering the SAXS and nitrogen adsorption-desorption results, the quantities of P123 and aluminum tri sec butoxide have been fixed to 3 and 4g, respectively, to investigate the effect of the amount of both the HCl and the citric acid on the properties of the mesostructured alumina.
Keeping the amount of citric acid at 0.5 g, for an HCl content less than 1 g or greater than 2 g, no reflection line is detected on the SAXS pattern (Fig. S4Aa), meaning that materials adopt a completely random pores network. The corresponding nitrogen adsorption-desorption isotherms are rather type II (Fig. S4Ab) and no maximum (2.5 g and 3 g of citric acid) or large pore size distribution with very low dV/dD value are observed (Fig. S4Ac). In that case, in the absence of hydrochloric acid, or at a low amount, it is difficult to control the reactivity of the alumina precursor and no mesostructure is formed. For 1 g of HCl the appearance, around 19.4 nm, of a not very intense broad peak on the SAXS pattern (Fig. S4Aa), indicates that the mesostructuration begins. The isotherm is type IV (Fig. S4Ab) with a H_1 hysteresis loop in accordance with the wormhole-like mesostructure evidenced by SAXS. The pore size distribution is very broad (Fig. S4Ac). When 1.5 g of hydrochloric acid are introduced, the HMS structure is observed (2 diffraction peaks). The synergic effect of HCl and citric acid for mesostructuration seems to be maximum. When the content in HCl increases to 2 g, the broad peak at 5.2 nm is no longer visible on the SAXS pattern, and the broad peak at 10.3 nm reflects the formation of a wormhole-like mesostructured. Isotherms are type IV with a H_1 loop, indicating an increase in the pore volume (Fig. S4Ab). The corresponding mesopores size distributions are more homogeneous (Fig. S4Ac). In this situation, the chloride ions are in excess and since they coordinate strongly with the aluminum ions, they disturb the porogen agent-inorganic precursor interactions.
Fixing the quantity of hydrochloric acid to 1.5 g, a similar trend is noted by varying the amount of citric acid (Fig. S2B). Nevertheless, the negative effect of the variation of the amount of citric acid on the specific surface area and on the pore volume is more pronounced than for HCl. Indeed, S_{BET} and V_P abruptly decrease from 400 to 37 m^2/g and from 0.87 to 0.05 cm^3/g, respectively, when the mass of citric acid is raised from 0.5 to 1.5 g (Fig. 1). Without citric acid,

the presence of Cl^- ions disrupts the self-assembly mechanism because they strongly coordinate with aluminum ions and, as explained above, a part of HCl is volatilizes, causing a rapid change in acidity of the medium and thereby making it more difficult to control the alumina precursor condensation. On the other hand, if the quantity of citric acid is too high, the citrate ions will disturb the interactions between the porogen agent and the inorganic precursor since these ions present in excess will interact with the P123 (salting out effect).
From Figure 1, which depicts the effect of each acid on the specific surface and on the pore volume, it can be conclude that there is an optimal mass of 1.5 g of hydrochloric acid and 0.5 g of citric acid that leads to the highest values of specific surface (400 m²/g) and pore volume (0.87 cm^3/g).

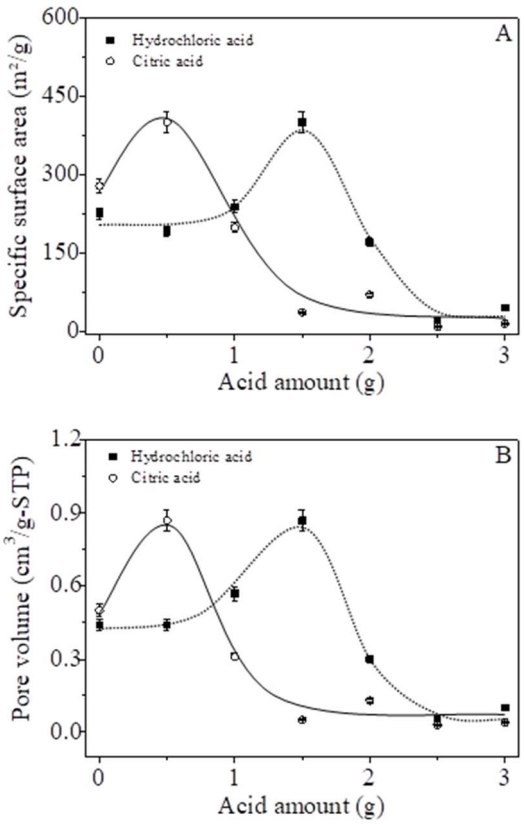

Figure 1: Variation of the specific surface area (A) and of the pore volume (B) as a function of the amount of both HCl and citric acid. Lines are just a guide for the eyes.

3.2. Efficiency of surfactant removal

According to the results reported above the best mesostructured alumina with an HMS mesopores arrangement has been synthesized using 3 g of P123, 4g of aluminum tri sec butoxide in the presence of 1.5 g of hydrochloric acid and 0.5 g of citric acid. The mesostucturation is further confirmed by TEM (Fig. S5A). After extraction of the porogen agent by Soxhlet using ethanol as solvent, a specific surface area of 403 m²/g, a pore volume of 0.83 g/cm^3 (Table 1) and a narrow pore size distribution centered around 8.3 nm have been obtained by nitrogen adsorption-desorption analysis. From TEM it can also be deduced that the mesoporosity is truly internal and regular (Fig. S5A). The XRD pattern (Fig. S5B) is characteristic of amorphous alumina [56]. To evaluate the efficiency of the elimination of organic molecules during the extraction, the amorphous mesostructured alumina was analyzed by infrared spectroscopy. In the 2500-4000 cm^{-1} range (Fig. 2Aa), the IR spectrum of the as-

synthesized material (Fig. 2) presents vibrations at 2870, 2900, 2930, 2974 and 3030 cm^{-1}. They can be attributed to the C-H stretchings of CH_2 and CH_3 s of the P123 alkyl chains [57]. The broad bands located around 3460 and 3170 cm^{-1} can be assigned to the O-H groups stretching and the N-H stretching of NH_4Cl [58], which is likely formed during the treatment under NH_3 atmosphere from the chloride ions present in the medium, respectively. The formation of NH_4Cl is further confirmed by the EDX mapping and spectrum of an as-synthesized alumina particle (Fig. 3A and Fig. S6A). Traces of nitrogen and chlorine are clearly visible on the surface of the particle. The locations of these two elements are very close, supporting the formation of NH_4Cl. Considering the 800-2000 cm^{-1} domain (Fig. 2Ab), the vibration attributed to the CH, CH_2 and CH_3 bonds are observed from 846 to 935 cm^{-1}, from 1253 to 1350 cm^{-1} and at 1377 cm^{-1}, respectively [57]. Vibration arising from starching of C-C and C-O bonds and are detected between 1000 and 1200 cm^{-1} [57]. At 1403 cm^{-1} the symmetric deformation mode of NH_4^+ in NH_4Cl, the carbon–hydrogen (CH_3), the carbon-carbon (C–C) and the carbon-oxygen (C=O) deformations are observed [56,58]. No band in the 1700-1850 cm^{-1} domain, assignable to C=O stretching mode of free citric acid is detected [59], thus no free citric acid remains in the as-synthesized alumina. After extraction of the surfactant by Soxhlet, the vibrational bands of the porogen agent are still detected on the infrared spectra (Fig. 2A), but with less intensity, meaning that a part of the organic molecules has been removed. The vibrational band of the N-H bond is also still detected with a lower intensity, meaning that not all of the salt is removed. Elementary analysis shows that 33% of carbon and 39% of nitrogen which are initially contained in the hybrid mesophase still remains in the mesostructured alumina after Soxhlet extraction (Table 2). To develop a lower energy consumer and an eco-friendlier process, the salt and the organics have been also removed by water or ethanol at room temperature. After immersion times, varying from 1 to 48 h, samples were withdrawn from the solution. They were dried in air at 40°C for 24 h in an oven. The powders obtained were then characterized. After 1 hour of immersion in water or in ethanol, the first peak on the SAXS pattern is shifted from 11.2 to 10.1 (Fig. S7A) or 10.3 nm (Fig. S7B), respectively. Increasing the immersion time, no significant change is noted in the SAXS pattern (Fig. S7). The contraction of the network is around 10% and it only occurs at the beginning of the extraction. Whatever the solvent and the immersion time a type IV isotherm with a H_1 hysteresis loop, characteristic of mesoporous materials is obtained (Fig. S8). However, the volume of adsorbed nitrogen is higher when ethanol is used instead of water. Performing the extraction with water, the specific surface area first increases during the first four hours of extraction. It goes from 228 to 374 m^2/g when the extraction time varies from 1 to 4 h, respectively. This suggest the formation of small boehmite particles due to the hydration of the surface [60]. For longer times, the specific surface area decreases, dropping from 365 m^2/g after 8 hours of extraction to 264 m^2/g after 48 h, likely because of the growth of the boehmite particles. The pore volume follows a similar trend to that of the specific surface (Table 2). With ethanol, the situation is quite different, after one hour of immersion, the specific surface and the pore volume are 391 m^2/g and 0.99 cm^3/g, respectively, and considering the error on the measurement, around 5%, both values remain almost constant when the immersion time is increased (Table 2). While no significant variation of the mesopore diameter is noted as a function of the immersion time when ethanol is used, the extraction by water leads to a slight decrease of its value (Table 2). For example, after 8 hours of immersion of water the mesopore diameter is 8.5 nm, whereas after the same time in ethanol its value is 9.8 nm. For a given time, ethanol also gives higher values of specific surface area of pore volume (Table 2). The difference of behavior is due to the hydration of the framework, which does not occur in presence of ethanol.

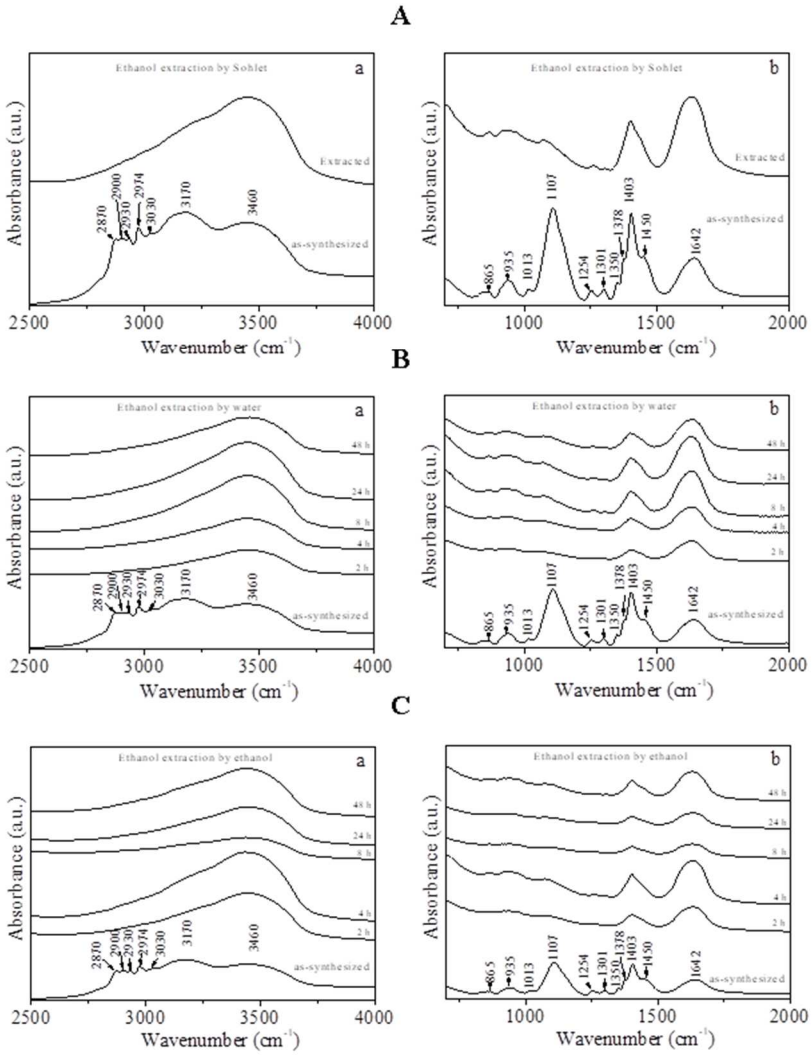

Figure 2: Infrared spectra in the 2500-4000 cm^{-1} (a) and 800-2000 cm^{-1} (b) ranges of the as-synthesized and the Soxhlet extracted alumina (A) and evolution of the infrared spectra with the extraction time by water (B) or ethanol (C) at room temperature.

Table 2: Variation of the specific surface area (S_{BET}), the pore volume (Vp), the mesopore diameter (∅), the percentage of carbon and nitrogen removed as a function of extraction time.

	Extraction time (h)	S_{BET} (m^2/g)	Vp (cm^3/g)	∅ (nm)	%C*	%N*
Immersion in water at room temperature	1	228	0.48	9.4	48	95
	2	357	0.84	9.7	44	93
	4	374	0.82	9.1	50	98
	8	269	0.55	8.5	50	95
	24	338	0.70	8.5	51	97
	48	264	0.53	8.3	48	94
Immersion in ethanol at room temperature	1	391	0.99	9.6	46	53.
	2	389	0.95	9.5	48	63
	4	409	1.06	9.8	47	79
	8	386	0.99	9.8	47	75
	24	445	1.11	9.7	47	75
	48	356	0.89	9.8	49	81
Ethanol extraction by Soxhlet	16	403	0.83	8.3	67	61

** Values determined by elementary analysis*

Whatever the solvent used, the vibrations of the organic compounds are attenuated but they are still visible, meaning that the extraction of the porogen agent is not complete (Fig. 2B and C). The Raman spectra reported in Figure S9 confirm that a part of the P123 molecules can be removed from the mesopores by water (Fig. S9A) or ethanol (Fig. S9B) extraction at room temperature. Indeed, a strong decrease of the bands assigned to alkyl chains of P123 at 1430 and 2800–3000 cm^{-1} [57] is noted after immersion in water (Fig. S9A) or in ethanol (Fig. S9B). Results obtained by elementary analysis shows that whatever the solvent, after 1 hour about 50% of carbon remain in the mesostructured alumina (Table 2). Increasing the immersion time until 48 hours does not modify this value (Table 2). After immersion during 2 hours in water, no chlorine signal is detected on the SEM-EDX mapping and a good dispersion of the nitrogen remaining on the particle is noted (Fig. 3B and Fig. S6B), indicating that NH_4Cl has been dissolved in water. This is further confirmed by the elementary analysis, which reveals that more than 90% of the initial nitrogen has been extracted from the material by water (Table 2). When ethanol is used, SEM-EDX mapping (Fig. 3C and Fig. S6C) always shows the presence of nitrogen and chlorine but the latter are better dispersed, indicating that a part of NH_4Cl is dissolved in ethanol. Elementary analysis shows that 50% of nitrogen is removed after 1 hour. Increasing the immersion time has a beneficial effect of nitrogen removal however it cannot be completely extracted and around 20% remain in the mesostructured alumina. Presence of residual carbon with an inhomogeneous distribution on the EDX mapping after water (Fig. 3B and Fig. S6B) or ethanol (Fig. 3C and Fig. S6C) extraction supports the fact that the organic compounds are only partially extracted.

3.3. Thermal stability of mesostructured Al_2O_3

Whatever the considered extraction method, the organic compounds are not completely eliminated and a calcination step is needed to release the porosity. This step can modify the properties of the mesostructured Al_2O_3, we have thus investigated its thermal stability. Since the highest percentage of carbon extraction has been obtained upon ethanol extraction by Soxhlet, this study has been carried out for mesostructured alumina obtained after Soxhlet extraction. From the SAXS pattern reported in Figure 4A, it can be deduced that the mesostructuration is maintained until 900°C. However, with the increase of temperature the broad peak observed at 10.3 nm for the extracted Al_2O_3 decreases in intensity and it becomes less resolved, meaning that the mesopore network is partially damaged. Its position is shifted from 10.3 to 7.1 nm after calcination at 500°C and to 6.3 nm after calcination at 900°C. This variation indicates a contraction of the mesopore network probably due to the partial crystallization of the amorphous walls and/or to the condensation of the surface aluminols. TEM images (Fig. S10) also evidenced that the mesopores network with a wormhole-like structure is maintained in this range of temperature. Above 900°C, no reflection line is detected anymore on the SAXS pattern (Fig. 4A), the mesostructure has completely collapsed. After calcination at 1000°C, many dark areas are observed on the surface of the particle by TEM (Fig. S10), they can indicate the crystallization of the walls. In addition, after calcination at 1000 or 1100°C no mesopore network can be seen from the TEM images (Fig. S10), confirming the mesostructure collapse. At 1100°C, the TEM image is composed of large zones, which can be attributed to an assemblage of alumina crystallites. Crystallization of the walls upon calcination is supported by the XRD analysis (Fig. 4B). The diffractograms of the materials calcined from 500 to 700 °C show amorphous materials. For calcination temperatures of 800 and 900°C, two reflections are visible at 2θ values of 45 and 67° corresponding respectively to the planes (400) and (440) of the γ-Al_2O_3 structure [56]. The peaks are of weak intensity and very widened, which reflects the presence of small crystallites. The crystallization of alumina correlates with the collapse of the mesostructure observed by SAXS.

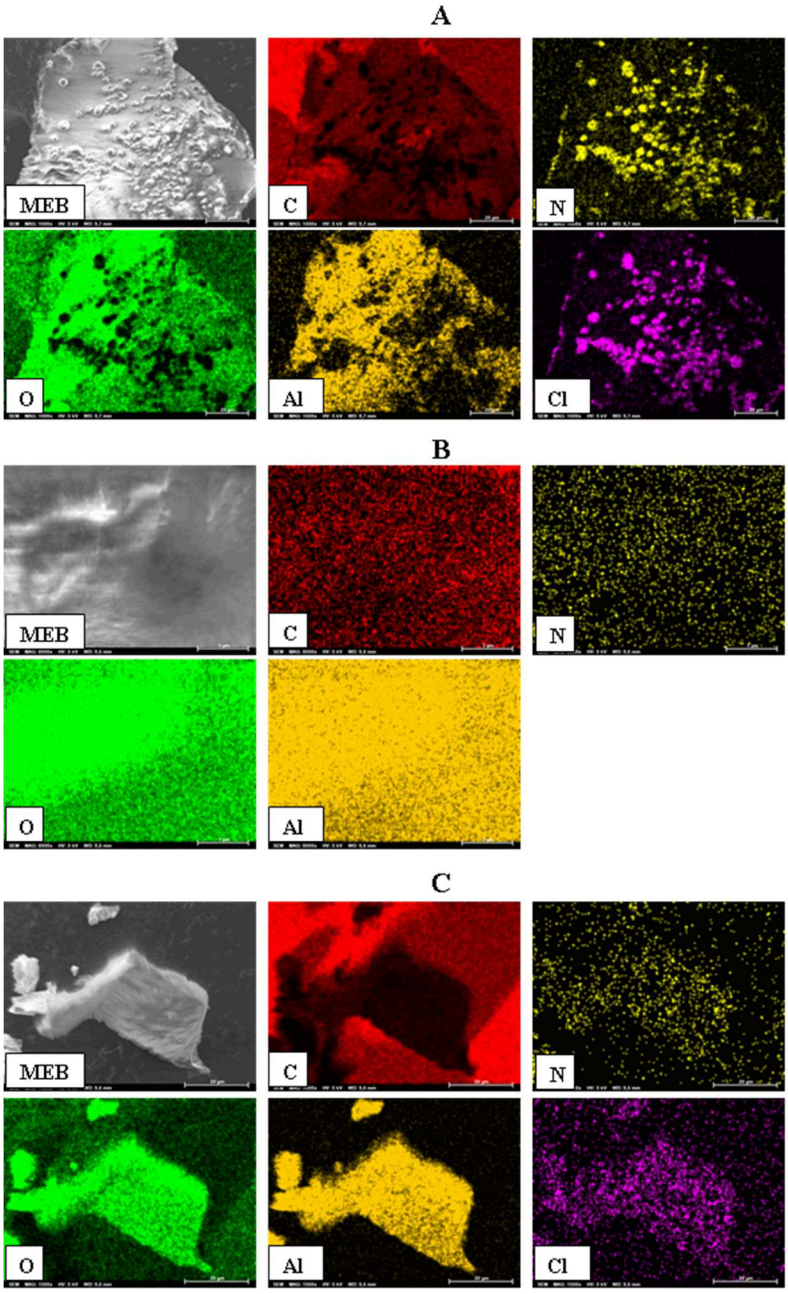

Figure 3: Energy dispersive X-ray analyses of the as-synthesized alumina (A) and of mesostructured alumina obtained after surfactant extraction during 2 hours at room temperature by water (B) or ethanol (C).

Increasing the temperature to 1000°C (Fig. 6B), the reflections at 2θ = 19, 32, 33, 37, 39, 45, 60 and 67° are assigned to the (013), (020) (022), (122), (026), (220), (232) and (042) planes of δ-Al_2O_3 [61]. The peaks are widened indicating the existence of small crystallites. After calcination at 1100°C (Fig. 4B), the diffractogram shows fine peaks reflecting the crystallization of the material. Traces of the δ-Al_2O_3 phase are still detected but, the dominant phase is α-Al_2O_3 characterized by the (012), (104), (110), (113), (024), (116), (214) and (300) planes situated at 2θ = 25, 35, 37, 43, 52, 57, 66 and 68°, respectively [56].
The type IV nitrogen adsorption-desorption isotherms are kept until a calcination temperature of 1000°C. However, increasing the temperature the hysteresis loop turns progressively from H_1 to H_2 and the volume of maximum adsorbed nitrogen decreases (Fig. 5A).

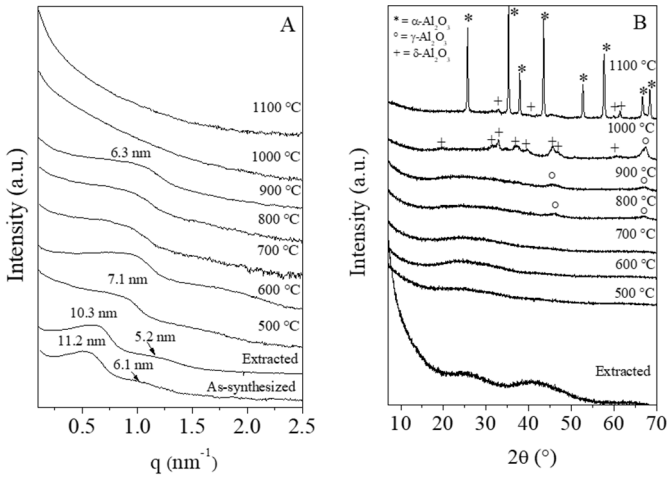

Figure 4: Variation of the SAXS (A) and XRD (B) patterns as a function of the calcination temperature.

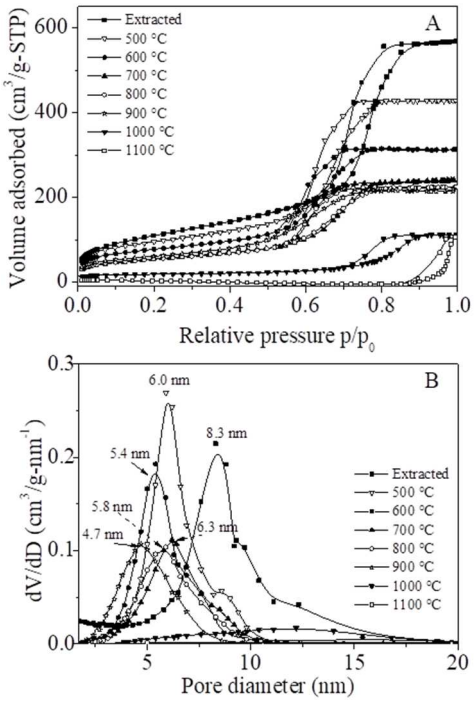

Figure 5: Variation of nitrogen adsorption-desorption isotherms (A) and pore size distribution (B) as a function of the calcination temperature.

For example, at saturation the volume of N_2 drops from 430 to 220 cm^3/g-STP if the calcination temperature is raised from to 500 to 900°C. Meantime, the mesopore size distribution becomes broader with a decrease of the dV/dD value and globally, its maximum is shifted towards lower value (Fig. 5B). For example, after calcination at 500°C the mean mesopore diameter is 6.0 nm whereas its value becomes 4.7 nm after calcination at 900°C (Table 3). These variations reflect the contraction of the mesopores network, its loss of homogeneity and the beginning of its collapse. The values of specific surface area and pore volumes of the materials decrease from 337 to 216 m²/g and from 0.65 to 0.33 cm^3/g, respectively when the temperature varies from 500 to 900°C (Table 3). After calcination at higher temperature the collapse of the mesostructured is more pronounced, resulting in lower specific surface and leading to non-porous solids with total collapse of the mesostructure after calcination at 1100°C due to the crystallization of the walls as observed by XRD.

Table 3: Variation of the specific surface area (S_{BET}), the pore volume (Vp), the mesopore diameter (∅), the percentage of carbon and nitrogen removed as a function of the calcination temperature.

Calcination Temperature (°C)	S_{BET} (m²/g)	Vp (cm^3/g)	∅ (nm)	%C*	%N*
500	337	0.65	6.0	96.6	> 98
600	274	0.48	5.4	> 99.9	> 99.9
700	194	0.36	6.3	> 99.9	> 99.9
800	193	0.34	5.8	> 99.9	> 99.9
900	216	0.33	4.7	> 99.9	> 99.9
1000	62	0.17	-	> 99.9	> 99.9
1100	6	0.05	-	> 99.9	> 99.9
Extracted	403	0.83	8.3	67	61

* Values determined by elementary analysis

In that case a type II isotherm is obtained (Fig. 5A) and no maximum is noted in the mesopore size distribution (Fig. 5B). Nevertheless, a residual interparticle porosity persists after calcination at 1000°C. It should be noted that after calcination at 500°C almost all the organic compounds and the salt are removed. Indeed, from elementary analysis it can be seen that around 4% and less than 2% of carbon and nitrogen, respectively, remain in the amorphous mesostructured alumina.

Modifying the calcination temperature also leads to a modification of the aluminum environment (Fig. 6). Indeed, ^{27}Al RMN spectra of material calcined at 500 to 700°C show the presence of three different environments for aluminum. Octahedral (AlO_6 ≈ 6.5 ppm), pentahedral (AlO_5 ≈ 37.4 ppm) and tetrahedral (AlO_4 ≈ 63 ppm) environments are detected [62,63]. The presence of these three contributions indicates a disordered aluminum organization, characteristic of an amorphous phase [64,65]. This observation is in coherence with SAXS and XRD analyses.

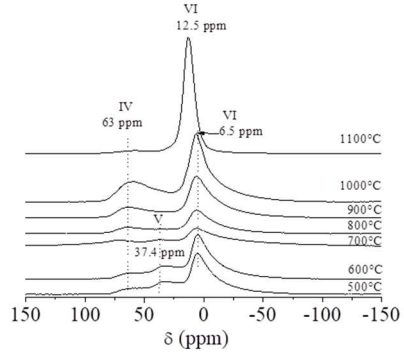

Figure 6: Variation of ^{27}Al NMR spectra as a function of the calcination temperature.

The materials calcined at 800, 900 and 1000 °C contain aluminum atoms with tetrahedral and octahedral coordinations, which is in accordance with the appearance γ-Al_2O_3 and δ-Al_2O_3 polymorphs detected by XRD [64,66]. Since both phases have similar Al environment it is not possible to distinguish them by ^{27}Al NMR [65]. After calcination at 1100°C, the resonance peaks assigned to Al in the octahedral environment is shifted from 6.5 to 12.5 ppm. This variation confirms the appearance of the α-Al_2O_3 structure [67], which contains only octahedral

aluminum [65]. The weak resonance at 63 ppm (Al in tetrahedral environment) can be attributed to the remaining δ-Al_2O_3, as observed by XRD.

3.4. Hydrothermal stability of mesostructured Al_2O_3

Hydrothermal stability is an important property that should be considered before developing applications, especially in catalysis. To evaluate this property, the mesostructured alumina has been first directly immersed in boiling water for 24 hours. Aliquots were taken at regular intervals and analyze. Secondly, the materials were exposed to water vapor at 200°C for 24 h. Since the environment of aluminum is modified with the increasing temperature of the calcination, this study has been performed by considering mesostructured alumina calcined at 500, 700 and 900°C. When immersed in boiling water or exposed to H_2O vapor, no reflection line is detected on the SAXS pattern of the mesostructured alumina calcined at 500°C (Fig. S11A) or 700°C (Fig. S11B). In that case, the mesostructured collapses even after 30 minutes in boiling water. The behavior after immersion in boiling water is quite different for the sample initially calcined at 900°C. Indeed, the broad peak at 6.4 nm can still be distinguished after 4 hours of immersion in boiling water (Fig. S11C). Initially, the nitrogen adsorption-desorption isotherms of all materials showed a sharp capillary condensation, after 0.5 h of immersion in boiling water this sharpness is drastically reduced. The hysteresis loop becomes H_2. However, while it still persists after 24 hours of immersion in boiling water for the mesostructured alumina calcined at 500°C (Fig. 7A), it completely disappears after 9 hours or 4 hours of treatment of the mesostructured aluminas calcined at 700°C and at 900°C, respectively, and a H_3 hysteresis loop is observed. In that latter cases, the samples exhibit an interparticular porosity. At the same time the isotherm is not type-IV anymore but rather type-II (Fig. 7B and C), according to the IUPAC classification, suggesting an interparticular porosity and the loss of the major part of the inner mesoporosity of the materials. This is further confirmed by the mesopore size distribution, which is very broad and presents low dV/dD values. After 24 hours in boiling water, the mesostructure collapses as observed for the other two materials.

The materials initially calcined at 500 and 700°C behave in a similar way after exposure to water vapor. Their nitrogen adsorption-desorption isotherm is rather type II (Fig. 7A and 7B), whereas the material calcined at 900°C shows a type IV isotherm with an H_3 type hysteresis after exposition to water vapor during 24 hours. The adsorption is therefore mainly interparticular. Anyway, whatever the calcination temperature of the started materials upon immersion in boiling water or after exposure to water vapor, the pore size distribution shows lower dV/dD values than the initial sample and it is also broader, reflecting the fact that the channels are progressively destroyed and that the mesostructure slowly collapses.

When tested in boiling water, whatever the temperature at which the initial mesostructured alumina is calcined, the specific surface area increased after immersion during 0.5 h. This can be attributed to the hydration of the framework, which leads to the formation of small particles of boehmite (γ-AlOOH) or pseudo bohemite [60, 68,69], depending on the calcination temperature of the initial mesostructured Al_2O_3. If the immersion time is prolonged, the values of the specific surface area remain almost constant for the material initially calcined at 500°C or decreases for the two other samples, presumably due to the growth of particles of (γ-AlOOH) [69]. The decrease of S_{BET} is accentuated with the increase in the calcination temperature (Fig. 8A). Considering the pore volume, if the starting alumina has been calcined at 500 or 700°C, its value decreases after the first 0.5 hour of immersion from 0.52 cm^3/ g to 0.40 cm^3/g and it remains almost constant thereafter (Fig. 8B). If the calcination has been performed at 900°C, the mesopore volume is constant around 0.35 cm^3/g during the first 2 hours of treatment in boiling water then it gradually drops to 0.19 cm^3/g after 24 hours (Fig. 8B). It appears that the impact of treatment in boiling water on the decrease in the specific surface area and in the pore volume values is more pronounced with the increase in the calcination temperature.

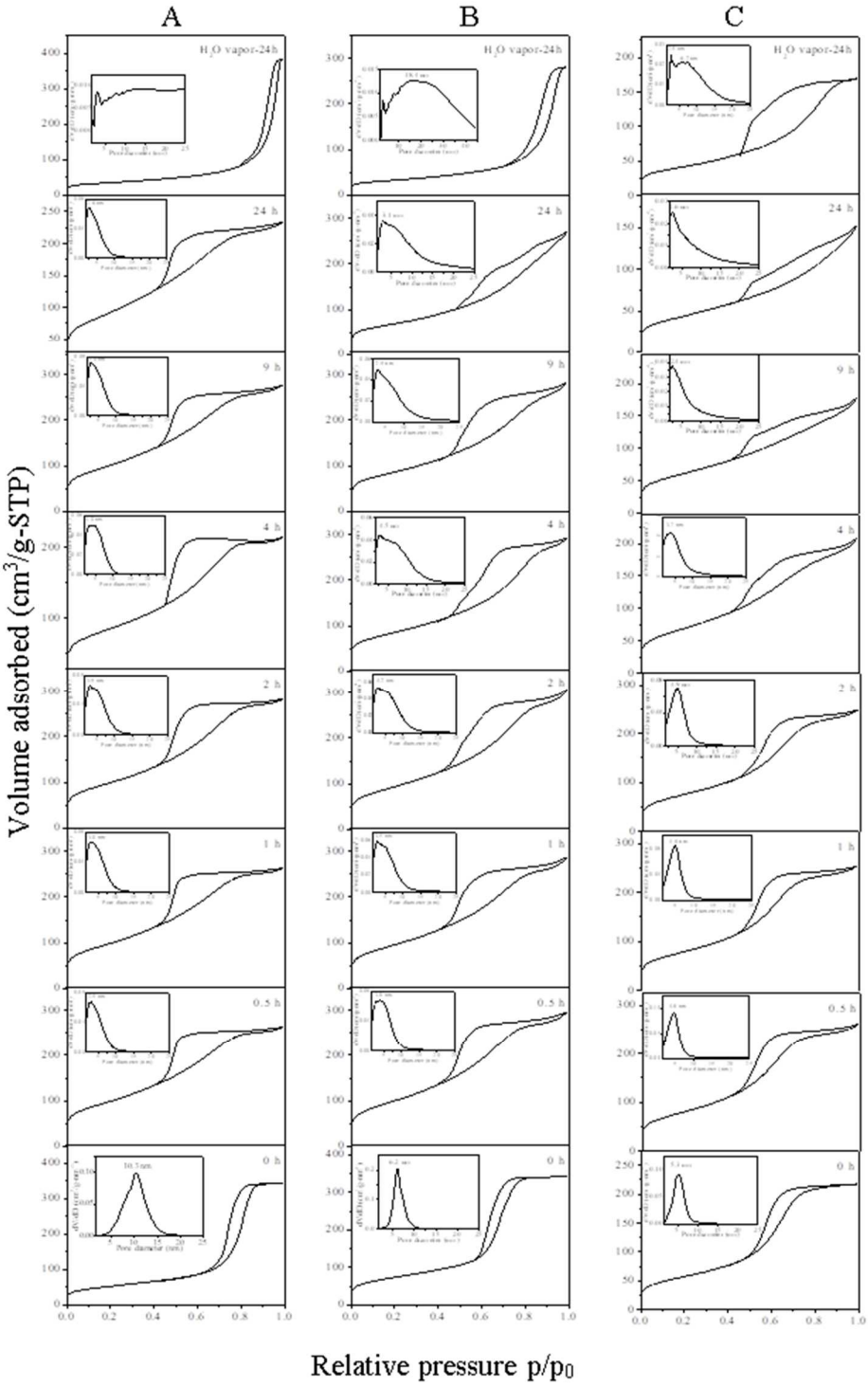

Figure 7: Nitrogen adsorption-desorption isotherms with the corresponding mesopores size distribution (insert) as a function of the immersion time in boiling water and after of exposure to water vapor. The initial mesostructured alumina has been calcined at 500°C (A), 700°C (B) or 900°C (C).

If the hydrothermal stability is evaluated by considering the exposure to water vapor during 24 hours, the drop of specific surface area is more important than for immersion in boiling water for materials calcined at 500 or 700°C. In fact, after 24 hours of exposure to water vapor S_{BET} is 122 and 149 m²/g, respectively, against 335 and 243 m²/g by considering the immersion in boiling water. The difference is much less significant, 149 versus 158 m²/g, when the material was initially calcined at 900°C.

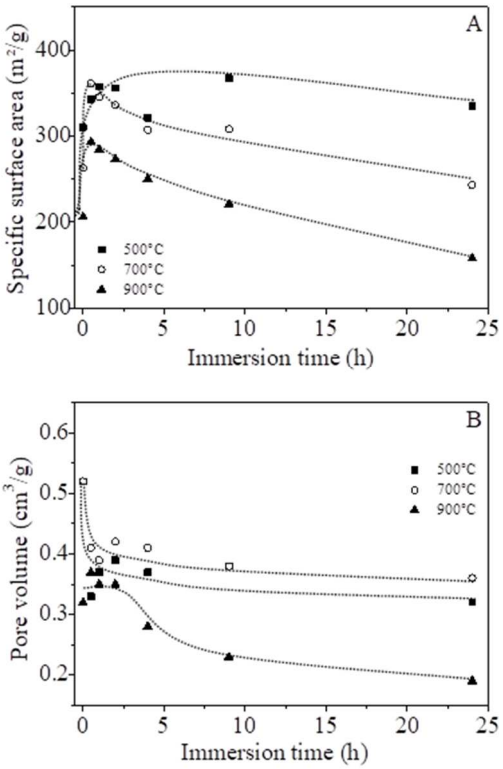

Figure 8: Variation of the specific surface area (A) and of the pore volume (B) with the immersion time in boiling water. The initial mesostructured alumina has been calcined at 500°C (■), 700°C (○) or 900°C (▲). Lines are just a guide for the eyes.

Figure 9 depicts the evolution of the XRD pattern of the calcined mesostructured alumina and after its immersion in boiling water during 24 hours or its exposure to water vapor during 24 hours. As observed previously, before immersion in boiling water or exposure to water vapor, materials calcined at 500 and 700°C are amorphous, no peak is detected on the XRD pattern. If calcination has been performed at 900°C only one peak at $2\theta = 45°$, which is assigned to the (400) reflection of γ-Al_2O_3 is observed. After 24 hours of immersion in boiling water, the XRD patterns of the mesostructured alumina show the presence of the (020), (120), (031), (200), (220) and (151) reflections of boehmite or pseudo-boehmite, depending on the heating temperature of the initial mesostructured alumina (Fig. 9). Indeed, the shift of the (020) reflections from $2\theta = 13.9$ to 14.5°, when the heating temperature is raised from 500 to 900°C, respectively, suggests that after 24 hours of immersion in boiling water pseudo boehmite is formed for the mesostructured Al_2O_3 initially calcined at 500°C (Fig. 9A). Whereas after the same period in boiling water boehmite is obtained for the material initially calcined at 900°C. XRD analysis thus confirms the presence of boehmite, which was assumed from the evolution of the specific surface area. In addition, for the sample initially heated at 900°C a more complex XRD pattern is obtained (Fig. 9C). Indeed, in addition to boehmite, the (010), (10-1), (-201), (-1-12) and (121) reflections of bayerite (JCPDS 01-074-1119) are detected at $2\theta = 18.6$, 21.1, 37.7, 39.9 and 45.0°, respectively. The (001), (110), (020), (011), (13-1), (22-1) and (13-2) reflections of nordstrandite (JCPDS 00-024-0006) appear at $2\theta = 18.9$, 20.4, 20.6, 21.4, 40.7, 45.7 and 50.2, respectively. The presence of these last two phases is consistent with the formation of γ-Al_2O_3 after calcination at 900°C. Indeed, the hydration of γ-Al_2O_3 also implies the formation of new phases according to the following equation [60] :

$$\gamma\text{-}Al_2O_3 + 3\ H_2O = 2\beta\text{-}Al(OH)_3$$

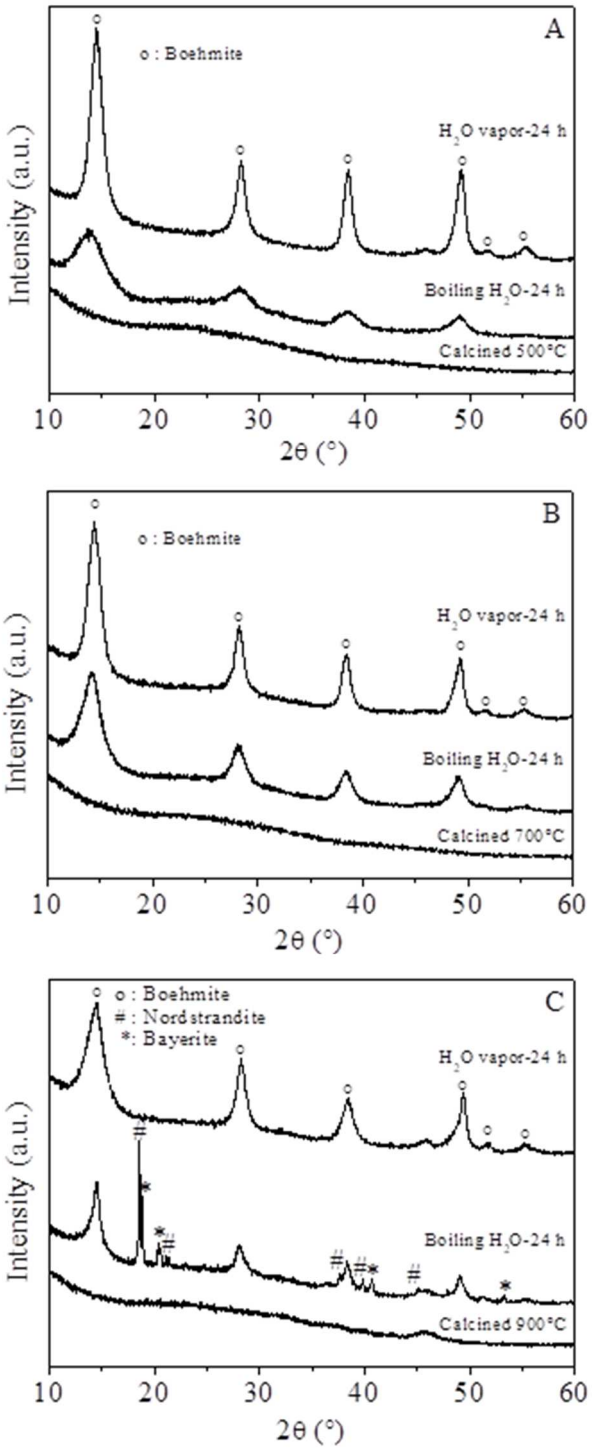

Figure 9: XRD pattern of the calcined mesostructured alumina and after its immersion in boiling water during 24 hours or its exposure to water vapor during 24 hours. The initial mesostructured alumina has been calcined at 500°C (A), 700°C (B) or 900°C (C).

The presence of bayerite and nordstrandite was also observed by Szűcs et al. during the rehydratation processes of heat-treated aluminium hydroxides in water vapor medium [70].
Evaluating the hydrothermal stability in presence of water vapor, after 24 hours of exposure, all XRD patterns present peaks at 14.5, 28.3, 38.5, 49.3, 51.6 and 55.3° which are respectively attributed to the (020), (120), (031), (200), (220) and (151) reflection of Boehmite (Fig. 9). Thus, after exposure for 24 hours to water vapor all the mesopore walls crystallize into boehmite

regardless of the calcination temperature, involving the collapse of the mesostructure. Additionally, compared to immersion in boiling water, a higher degree of crystallization, reflected by more intense diffraction peaks, is noted.
From the XRD results, it is reasonable to conclude that the collapse of the mesoporous framework is related to the crystallization of the amorphous walls.

4. Conclusions

Mesostructured amorphous Al_2O_3 has been synthesized in an alcoholic acidic media by a surfactant templating process using P123 as porogen agent and aluminum tri sec butoxide as alumina precursor. The role of ethanol, citric acid and hydrochloric acid is to control the reactivity of the alumina precursor. Chlorides and citrates ions are therefore present in the synthesis medium and depending on their quantity they can interact preferentially either with the surfactant or with the inorganic precursor, disrupting the interactions of aluminum species with the porogen agent. The influence of the synthesis conditions on the properties of mesoporous materials has been investigated. Results show that the best mesopore ordering is reached for 3g of porogen agent, 4g of aluminum tri sec butoxide, 0.5 of citric acid and 1.5g of HCl. However, even under these conditions only an HMS mesostructure is obtained. The reconstitution of the liquid crystal phase during the evaporation step is not complete likely because the presence of water, which favors the hydrolysis and thus affects the homogeneity of the particles. Probably, due to the salting out effect of citrates, dual mesoporous materials are obtained when the mesostructured alumina is synthesized from 1g of P123 in the presence of citric acid.
The partial release of porosity was carried out by water or ethanol extraction at room temperature. The results show that even after 48 hours 50% of the carbon present in the hybrid mesophase still remain. When extraction is performed with Soxhlet, the percentage of remaining carbon after 16 hours is 33%.
The investigation of the thermal stability shows that the mesostructure is maintained until 900°C, temperature at which the γ-Al_2O_3 appear. Increasing the temperature, the walls of the mesopores framework crystallize into δ-Al_2O_3 and finally into α-Al_2O_3. The crystallization process involves the collapse of the mesostructure.
The hydrothermal stability of mesostructured alumina calcined at 500, 700 and 900°C has been evaluated in boiling water or in the presence of water vapor. The results show that at the beginning of the treatment, due to the hydration of the Al_2O_3, small particles of boehmite are formed, involving an increase in the specific surface area. However, the crystallization into aluminum hydroxides involved the collapse of the mesostructure.
Comparing with literature, the preparation method reported here is eco-friendlier since it allows the partially template removal by water at room temperature. It also allows to preserve the presence of amorphous phase in the materials upon thermal treatment at 700°C. This open new opportunity for the design of CoMoS hydrotreating catalysts. Indeed, the presence of the amorphous phase can play an important role in enhancing the activity and durability of the catalysts because of its unique chemical properties (presence of defect, acidity, basicity….) which will affect the features of the active phase (size, morphology…). For the same reasons, the selectivity can also be modified. Undoubtedly, improved dispersion of the active phase can be achieved by integration into high surface area materials containing amorphous phase. In addition, one can expect that the interaction with Mo precursors and/or the MoS_2 slabs would be drastically modified. This work is still in progress and will be reported elsewhere.

Credit authorship contribution statement

Jean-Luc Blin: Writing - original draft, Supervision, Florian Jonas: Investigation, Laure Michelin: Investigation, Séverinne Rigolet: Investigation, Ludovic Josien: Investigation, Loïc Vidal: Investigation, Lionel Richaudeau: Investigation, Bénédicte Lebeau: Writing - original draft, Supervision.

Conflicts of interest
The authors declare that they have no competing interests

Acknowledgments
We would like to thank Sandrine Adach (L2CM) from the platform «SynBioN» for elementary analyses and Laurent Mori (L2CM) for the design of the home made glass support. Florian Jonas thanks the « Region Grand-Est » for the financial support of his PhD.

Funding:
This work was supported by the « Region Grand-Est » [grant number RPHPHXAS-D-AOT17-TITAN].

Appendix A. Supplementary data
SAXS pattern as a function of the amount of both P123 and aluminum tri sec butoxide. Materials have been prepared without addition (A) or in the presence (B) of citric acid (S1).
Nitrogen adsorption-desorption isotherms with the corresponding mesopores size distribution (insert) as a function of the amount of both P123 and aluminum tri sec butoxide. Materials have been prepared in the presence of citric acid (S2).
Nitrogen adsorption-desorption isotherms and mesopores size distribution as a function of the amount of both P123 and aluminum tri sec butoxide of materials prepared without addition of citric acid (S3).
SAXS patterns, nitrogen adsorption-desorption isotherms) and mesopores size distribution as a function of the amount of both HCl and citric acid (S4).
TEM images and XRD after surfactant extraction by Soxhlet (S5).
EDX spectra after surfactant extraction by water or ethanol at room temperature (S6).
SAXS patterns as a function of the surfactant extraction by water or ethanol with time at room temperature (S7).
Nitrogen adsorption-desorption isotherms and mesopores size distribution as a function of the surfactant extraction by water or ethanol with time at room temperature (S8).
Raman spectra as a function of the extraction by water or ethanol with time at room temperature (S9).
TEM images as a function of the calcination temperature (S10).
SAXS pattern as a function of the immersion time in boiling water and after exposure to water vapor (S11).

References

[1] H. Pines, W. Haag, Alumina-catalyst and support. I. Alumina, its intrinsic acidity and catalytic activity, J. Am. Chem. Soc. 82 (1960) 2471-2483.

[2] G. Busca, The surface of transitional aluminas: A critical review, Catal. Today 226 (2014) 2-13.

[3] C. Misra, Industrial alumina chemicals, ACS Monograph 184, Washington, 1986.

[4] H. Topsoe, B.S. Clausen, F.E. Massoth, Hydrotreating catalysis, Springer, Berlin, 1996, p. 310.

[5] A. N. Zagoruiko, V. V. Shinkarev, S. V. Vanag, G. A. Bukhtiyarova, Catalytic processes and catalysts for production of elemental sulfur from sulfur-containing gases, Catal. Ind. 2 (2010) 343-352.

[6] G. Busca, Structural, surface, and catalytic properties of aluminas, Adv. Catal. 57 (2014) 319-404.

[7] H. Knözinger, R. Köhne, he dehydration of alcohols over alumina. I. The reaction scheme, J. Catal. 5 (1966) 264-270.

[8] T. K. Phung, A. Lagazzo, M. Á. Rivero Crespo, V. Sánchez Escribano, G. Busca, A study of commercial transition aluminas and of their catalytic activity in the dehydration of ethanol, J. Catal. 311 (2014) 102-113.

[9] M. Zhang, Y. Yu, Dehydration of ethanol to ethylene, Ind. Eng. Chem. Res. 52 (2013) 9505-9514.

[10] A. Tanimu, K. Alhooshani, Advanced hydrodesulfurization catalysts: A review of design and synthesis, Energy Fuels 33 (2019) 2810-2838.

[11] I. Levin and D. Brandon, Metastable alumina polymorphs: crystal structures and transition sequences, J. Am.Ceram. Soc. 81 (2005) 1995-2012.

[12] M. Trueba, S.P. Trasatti, γ-alumina as a support for catalysts: a review of fundamental aspects, Eur. J. Inorg. Chem. 17 (2005) 3393-3403.

[13] S. K. Bej, S. K. Maity, U.T. Turaga, Search for an efficient 4,6-DMDBT hydrodesulfurization catalyst: A Review of recent studies, Energy Fuels 5 (2004) 1227-1237.

[14] F. Bataille, J.L. Lemberton, P. Michaud, G. Pérot, M. Vrinat, M. Lemaire, E. Schulz, M. Breysse, S. Kasztelan, Alkyldibenzothiophenes hydrodesulfurization-promoter effect, reactivity, and reaction mechanism, J.Catal. 191 (2000) 409-422.

[15] C. Bara, L. Plais, K. Larmier, E. Devers, M. Digne, A.F. Lamic-Humblot, G.D. Pirngruber, X. Carrier, Aqueous-phase preparation of model HDS catalysts on planar alumina substrates: support effect on Mo adsorption and sulfidation, J. Am. Chem. Soc. 2015, 137, 15915-15928.

[16] A. Miño, C. Lancelot, P. Blanchard, C. Lamonier, L. Rouleau, M. Roy-Auberger, S. Royer, E. Payen, Strategy to produce highly loaded alumina supported CoMo-S catalyst for straight run gas oil hydrodesulfurization, Appl. Catal., A 530(2017) 145-153.

[17] C. Márquez-Alvarez, N. Žilková, J. Pérez-Pariente, J. Čejka, Synthesis, characterization and catalytic applications of organized mesoporous aluminas, Catal. Rev. 50 (2008) 222-286.

[18] H. Liu, Y. Zhang, L. Lv, X. Gao, H. Meng, H. Liu, Obtaining of mesoporous aluminosilicates with high hydrothermal stability by composite organic templates: utility and mechanism, Langmuir 37 (2010) 9137-9143.

[19] Y. Deng, J. Zhou, G. Li, H. Liu, X. Gao, Y. Yue, H. Li, F. Xie, H. Liu, Synthesis of well-ordered mesoporous aluminosilicates with high aluminum contents: the challenge and the promise, Inorg. Chem. 61 (2022) 11820-11829.

[20] H. Chen, F. Zhen, H. Liu, X. Gao, Y. Yue, H. Liu, H. Liu, Hydrophobic polypropylene glycol integration into the micelles: a general approach for high utilization efficiency of organic template, Ind. Eng. Chem. Res. 60 (2021) 9482-9488.
[21] Y. Deng, J. Wei, Z. Sun, and D. Zhao, Large-pore ordered mesoporous materials templated from non-Pluronic amphiphilic block copolymers, Chem. Soc. Rev. 42 (2013) 4054-4070. 2013.
[22] D Gu, F. Schüth, Synthesis of non-siliceous mesoporous oxides, Chem. Soc. Rev. 43 (2014) 43 313-344
[23] R. Ryoo, S.H. Joo, S. Jun, Synthesis of highly ordered carbon molecular sieves via template-mediated structural transformation, J. Phys. Chem. B 103 (1999) 7743-7746.
[24] T. Kimura, Evaporation-induced self-assembly process controlled for obtaining highly ordered mesoporous materials with demanded morphologies, Chem. Rec. 16 (2016) 445-457.
[25] M.B. Bahari, C.R. Mamat, A.A. Jalil, N.S. Hassan, W. Nabgan, H.D. Setiabudi, D.V.N. Vo, B.T.P. Thuy, Mesoporous alumina: A comprehensive review on synthesis strategies, structure, and applications as support for enhanced H_2 generation via CO_2-CH_4 reforming, Int. J. Hydrogen Energy 47 (2022) 41507-41526.
[26] S. Haffer, C. Weinberger, M. Tiemann, "Mesoporous Al_2O_3 by nanocasting: Relationship between crystallinity and mesoscopic order, Eur. J. Inorg. Chem., 20 (2012) 3283-3288.
[27] Q. Liu, A. Wang, X. Wang, T. Zhang, Ordered crystalline alumina molecular sieves synthesized via a nanocasting route, Chem. Mater. 18 (2006) 5153-5155.
[28] M. Yada, M. Machida T. Kijima, Synthesis and deorganization of an aluminium–based dodecyl sulfate mesophase with a hexagonal structure, Chem. Commun. 6 (1996) 769-770.
[29] P. Yang, D. Zhao, D. I. Margolese, B. F. Chmelka, G. D. Stucky, Block copolymer templating syntheses of mesoporous metal oxides with large ordering lengths and semicrystalline framework, Chem. Mater. 11 (1999) 2813-2826.
[30] A. Caragheorgheopol, H. Caldararu, G. Ionita, F. Savonea, N. Žilková, A. Zukal, J. Čejka, Solvent-induced textural changes of as-synthesized mesoporous alumina, as reported by spin probe electron spin resonance spectroscopy, Langmuir 21 (2005) 2591-2597, 2005.
[31] K. Niesz, P. Yang, G. A. Somorjai, Sol-gel synthesis of ordered mesoporous alumina, Chem. Commun. 15 (2005) 1986-1987.
[32] C. Boissière, L. Nicole, C. Gervais, F. Babonneau, M. Antonietti, H. Amenitsch, C. Sanchez, D. Grosso, Nanocrystalline mesoporous γ-alumina powders "UPMC1Material" gathers thermal and chemical ctability with high surface area, Chem. Mater. 18 (2006) 5238-5243.
[33] Q. Yuan, A.X. Yin, C. Luo, L.D. Sun, Y.W. Zhang, W.T. Duan, H.C. Liu, C.H. Yan, Facile synthesis for ordered mesoporous γ-Aluminas with high thermal stability, J. Am. Chem. Soc. 130 (2008) 3465-3472.
[34] P. F. Fulvio, R. I. Brosey, M. Jaroniec, Synthesis of mesoporous alumina from boehmite in the presence of triblock copolymer," ACS Appl. Mater. Interfaces, 2 (2010) 588-593.
[35] R. Bleta, P. Alphonse, L. Pin, M. Gressier, M. J. Menu, An efficient route to aqueous phase synthesis of nanocrystalline γ-Al_2O_3 with high porosity: From stable boehmite colloids to large pore mesoporous alumina, J. Colloid Interface Sci. 367 (2012) 120-128.
[36] W. Wu, Z. Wan, W. Chen, M. Zhu, D. Zhang, Synthesis of mesoporous alumina with tunable structural properties, Microporous Mesoporous Mater. 217 (2015) 12-20.

[37] W. Wu, Z. Wan, M. Zhu, D. Zhang, A facile route to aqueous phase synthesis of mesoporous alumina with controllable structural properties, Microporous Mesoporous Mater. 223 (2016) 203-212.
[38] X. Xu, S.K. Megarajan, Y. Zhang, H. Jiang, Ordered mesoporous alumina and their composites based on evaporation induced self-assembly for adsorption and catalysis, Chem. Mater. 32 (2020) 3-26.
[39] A.A.S. Gonçalves, M.J.F. Costa, L. Zhang, F. Ciesielczyk, M. Jaroniec, One-Pot Synthesis of MeAl2O4 (Me = Ni, Co, or Cu) supported on γ-Al_2O_3 with ultralarge mesopores: enhancing interfacial defects in γ-Al_2O_3 to facilitate the formation of spinel structures at lower temperatures, Chem. Mater. 30 (2018) 436-446.
[40] Z. Zhang, S. Yang, X. Hu, H. Xu, H. Peng, M. Liu, B.P. Thapaliya, K. Jie, J. Zhao, J. Liu, H. Chen, Y. Leng, X. Lu, J. Fu, P. Zhang, S. Dai, Mechanochemical nonhydrolytic sol−gel-strategy for the production of mesoporous multimetallic oxides, Chem. Mater. 31 (20189 5529-5536.
[41] E. Weidner, R. Dubadi, B. Samojeden, A. Piasecki, T. Jesionowski, M. Jaroniec, F. Ciesielczyk, Mechanochemical synthesis of alumina-based catalysts enriched with vanadia and lanthana for selective catalytic reduction of nitrogen oxides, Sci. Rep. 12 (2022):21294.
[42] K. Zimny, T. Roques-Carmes, C. Carteret, M. J. Stébé J. L. Blin, Synthesis and photoactivity of ordered mesoporous titania with a semicrystalline framework, J. Phys. Chem. C 116 (2012) 6585-6594.
[43] B. Lebeau, I. Naboulsi, L. Michelin, C. Marichal, S. Rigolet, C. Carteret, S. Brunet, M. Bonne, J.L. Blin, RSC Adv., 10 (2020) 26165-26176.
[44] I. Naboulsi, C. F. Linares Aponte, B. Lebeau, S. Brunet, L. Michelin, M. Bonne J. L. Blin, An unexpected pathway for hydrodesulfurization of gazole over a CoMoS active phase supported on a mesoporous TiO_2 catalyst, Chem. Commun. 53 (2017) 2717-2720.
[45] I. Naboulsi, B. Lebeau, C. F. Linares Aponte, S. Brunet, M. Mallet, L. Michelin, M. Bonne, C. Carteret, J.L. Blin, Selective direct desulfurization way (DDS) with CoMoS supported over mesostructured titania for the deep hydrodesulfurization of 4,6-dimethydibenzothiophene, Appl. Catal., A 563 (2018) 91-97.
[46] M. Thommes, K. Kaneko, A. V. Neimark, J. P. Olivier, F. Rodriguez-Reinoso, J. Rouquerol, K. S. W. Sing, Physisorption of gases, with special reference to the evaluation of surface area and pore size distribution (IUPAC Technical Report), Pure Appl. Chem. 87 (2015) 1051-1069.
[47] S.A. Bagshaw, E. Prouzet, T.J. Pinnavaia, Templating of mesoporous molecular sieves by nonionic polyethylene oxide surfactants, Science 269 (1995) 1242-1244.
[48] E. Prouzet, T.J. Pinnavaia, Assembly of mesoporous molecular sieves containing wormhole motifs by a nonionic surfactant pathway: control of pore size by synthesis temperature, Angew. Chem. Int. Ed. Engl. 36 (1997) 516-518.
[49] P.T. Tanev, M. Chibwe, T.J. Pinnavaia, T. Titanium-containing mesoporous molecular sieves for catalytic oxidation of aromatic compounds, Nature 368 (1994) 321-323.
[50] P.T. Tanev, T.J. Pinnavaia, Mesoporous silica molecular sieves prepared by ionic and neutral surfactant templating: A comparison of physical properties, Chem. Mater. 8 (1996) 2068-2079.
[51] S. S. Soni, G. Brotons, M. Bellour, T. Narayanan, A. Gibaud, Quantitative SAXS analysis of the P123/water/ethanol ternary phase diagram, J. Phys. Chem. B 110 (2006) 15157- 15165.
[52] K. Assaker, I. Naboulsi, M.J. Stébé, M. Emo, J.L. Blin, Investigation of mixed fluorinated and triblock copolymer liquid crystals: Imprint for mesostructured bimodal silica, J. Colloid Interface Sci. 446 (2015) 170-176.

[53] W Wu, M. Zhu, D. Zhang, The role of solvent preparation in soft template assisted synthesis of mesoporous alumina, Microporous Mesoporous Mater. 260 (2018) 9-16.
[54] K.P. Gregory, G.R. Elliott, H. Robertson, A. Kumar, E.J. Wanless, G.B. Webber, V.S. J. Craig, G.G. Andersson, A.J. Page, Understanding specific ion effects and the Hofmeister series, Phys. Chem. Chem. Phys. 24 (2022) 12682-12718.
[55] F. Michaux, J.L. Blin, M.J. Stébé, Relation between the lower consolute boundary and the structure of mesoporous silica materials, Langmuir 24 (2008) 1044-1052.
[56] J. Gangwar, B.K. Gupta, S.K. Tripathi, A. K. Srivastava, Phase dependent thermal and spectroscopic responses of Al_2O_3 nanostructures with different morphogenesis, Nanoscale 7 (2015) 13313-13344.
[57] C.G.H. Liu, J. Wang, J. Chen, Conformational structure of triblock copolymersby FT-Raman and FTIR spectroscopy, J Colloid Interface Sci. 209 (1999) 368-73.
[58] K. Nakamoto, Infrared and Raman spectra of inorganic and coordination compounds. Part A: Theory and applications in inorganic chemistry, fifth ed., Wiley, New York, 1997.
[59] Z. Hua-Min, T. Yasutake, Y. Noboru, Preparation of perovskite-type oxides with large surface Aarea by citrate process, Chem. Lett. 16 (1987) 665-668.
[60] G. Lefèvre, M. Duc, P. Lepeut, R. Caplain, M. Fédoroff, Hydration of γ-alumina in water and its effects on surface reactivity, Langmuir 18 (2002) 7530-7537.
[61] Y. Repelin, E. Husson, Etudes structurales d'alumines de transition. I-Alumines gamma et delta, Mat. Res. Bull. 25 (1990) 611-621.
[62] H. Hashimoto, K. Yazawa, H. Asoh, S. Ono, NMR spectroscopic analysis of the local structure of porous-type amorphous alumina prepared by anodization, J. Phys. Chem. C 121 (2017) 12300-12307, 2017.
[63] J. Čejka, Organized mesoporous alumina: Synthesis, structure and potential in catalysis, Appl. Catal., A 254 (2003) 327-338.
[64] T.R. Lopes, G.R. Gonçalves, E. de Barcellos Jr., M.A. Schettino Jr., A.G. Cunha, F.G. Emmerich, J.C.C. Freitas, Solid state 27 Al NMR and X-ray diffraction study of alumina–carbon composites, Carbon 93 (2015) 751-761.
[65] P. Kaur, A. Khanna, N. Kaur, P. Nayar, B. Chen, Synthesis and structural characterization of alumina nanoparticles, Phase Transitions 93 (2020) 596-605.
[66] M.H. Lee, C.F. Cheng, V. Heine, J. Klinowski, Distribution of tetrahedral and octahedral Al sites in gamma alumina, Chem. Phys. Lett. 265 (1997) 673-676.
[67] C. Pecharromán, I. Sobrados, J.E. Iglesias, T. González-Carreño, J. Sanz, Thermal evolution of transitional aluminas followed by NMR and IR Spectroscopies, J. Phys. Chem. B 103 (1999) 6160-6170.
[68] M. W. Hahn, J.R. Copeland, A.H. van Pelt, C. Sievers, Stability of amorphous silica-alumina in hot liquid water, ChemSusChem 6 (2013) 2304-2315.
[69] R. M. Ravenelle, J. R. Copeland, W.G. Kim, J.C. Crittenden, C. Sievers, Structural changes of γ-Al_2O_3-supported catalysts in hot liquid water, ASC Catal. 1 (2011) 552-561.
[70] V.Z. Baranyai, F. Kristály, I. Szűcs, Low temperature rehydration of thermally dehydroxylated Bayer–gibbsite, evolution and transformation of phases, J. Therm. Anal. Calorim. 129 (2017) 1353-1365.

Supporting Information

Figure S1: Evolution of the SAXS pattern as a function of the amount of both P123 and aluminum tri sec butoxide. Materials have been prepared without addition (A) or in the presence (B) of citric acid.

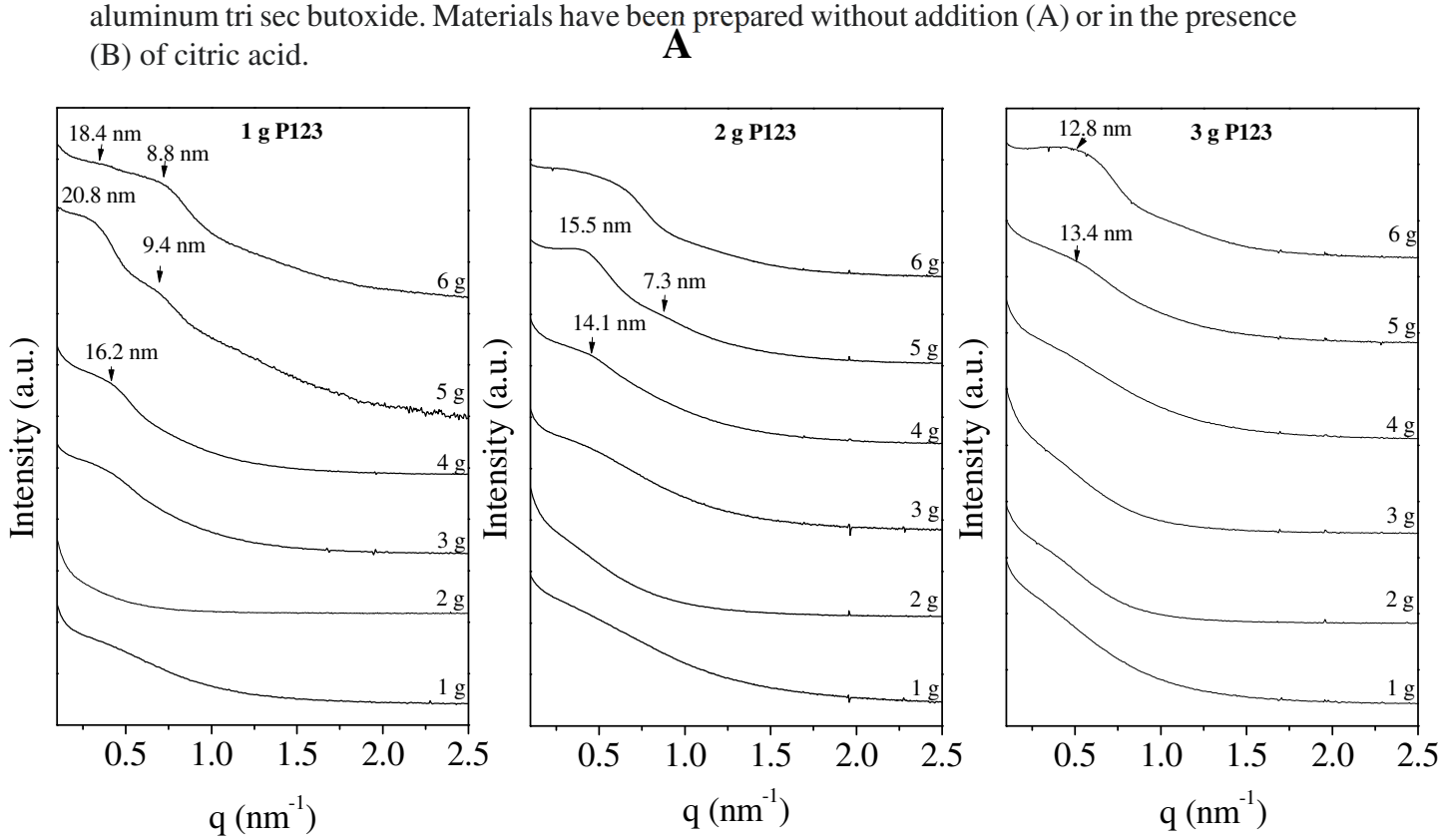

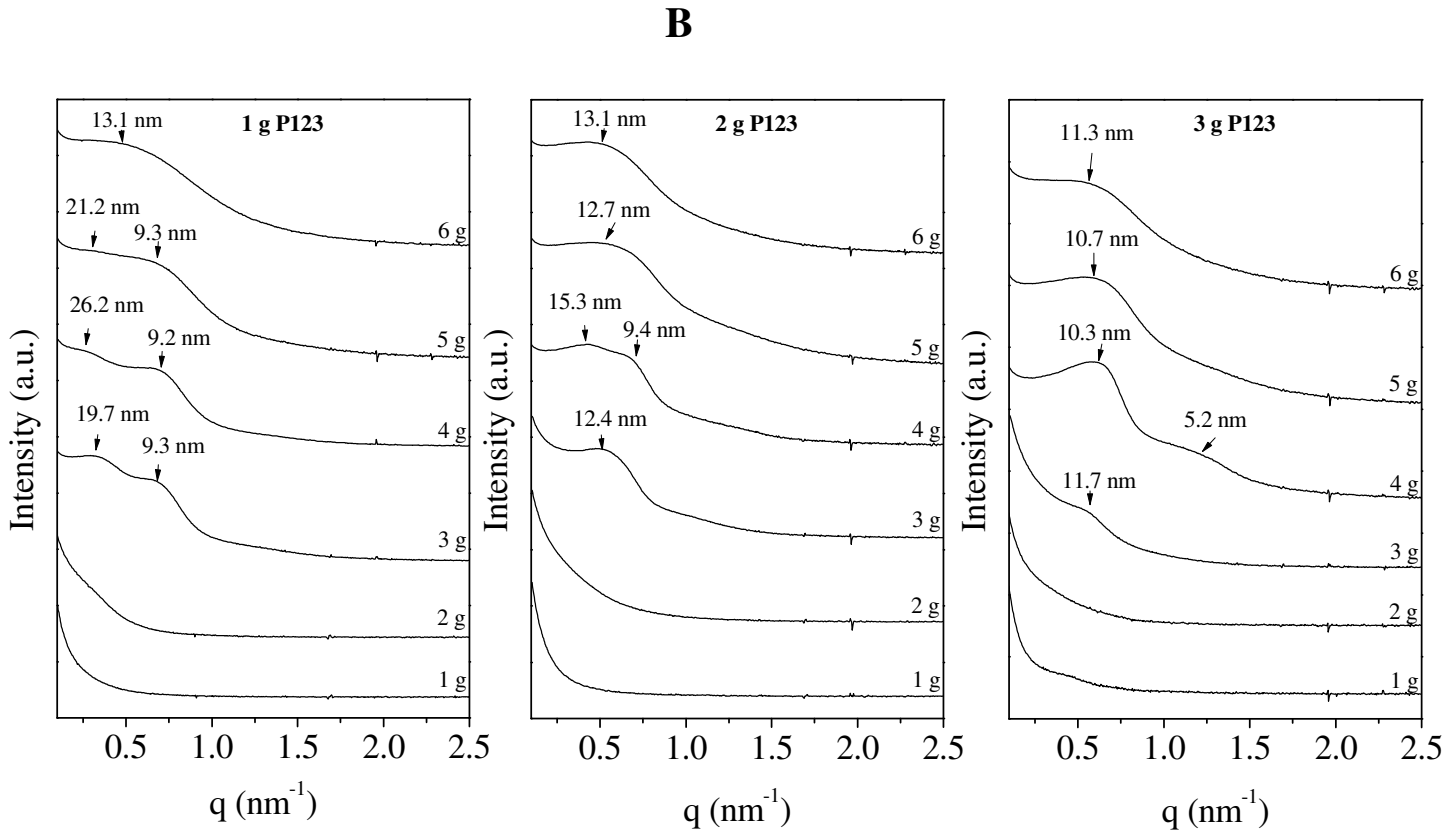

Figure S2: Variation of the nitrogen adsorption-desorption isotherms with the corresponding mesopores size distribution (insert) as a function of the amount of both P123 and aluminum tri sec butoxide. Materials have been prepared in the presence of citric acid with 1 (A), 2 (B) and 3 (C) g of P123.

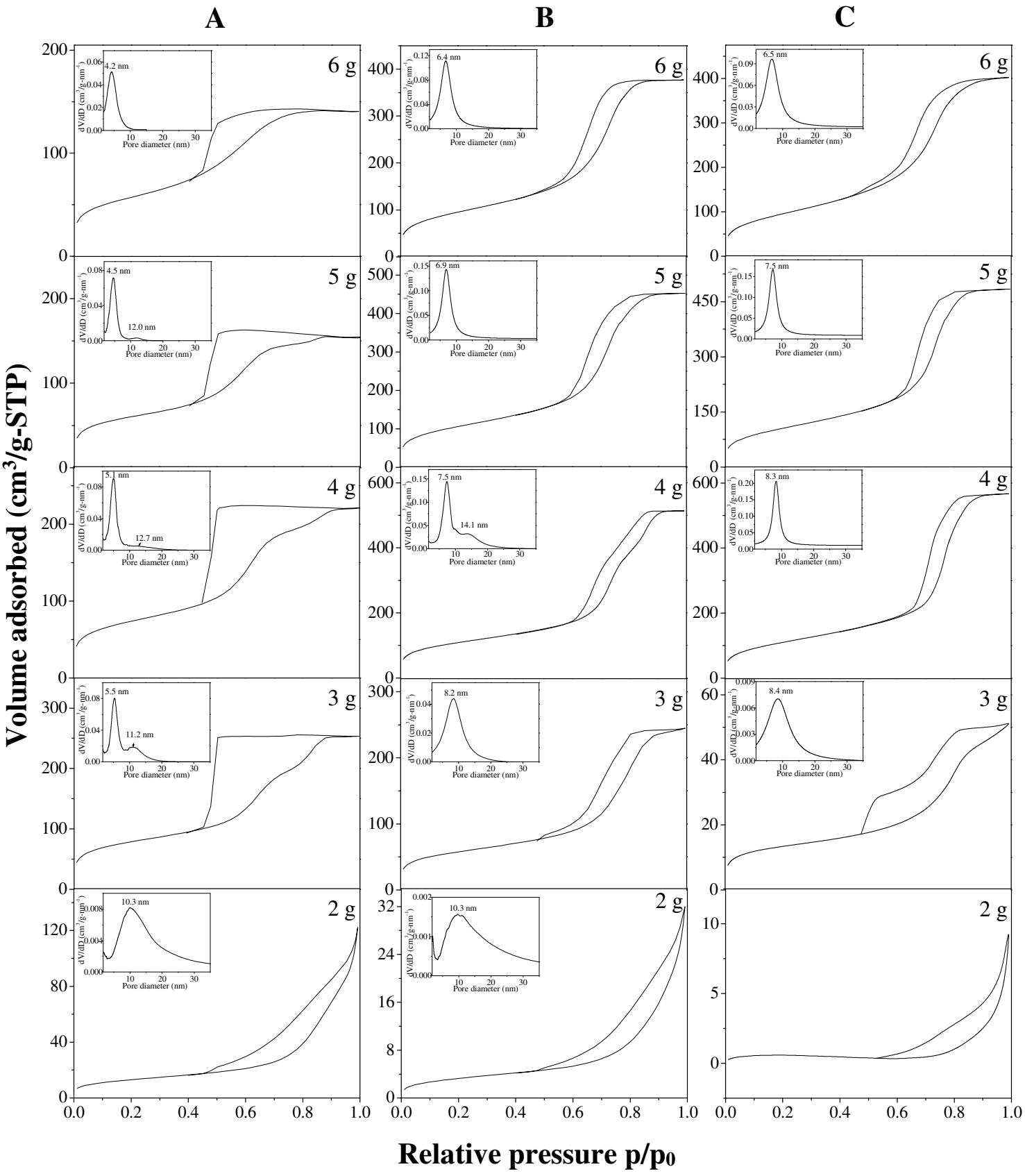

Figure S3: Variation of the nitrogen adsorption-desorption isotherms with the corresponding mesopores size distribution (insert) as a function of the amount of both P123 and aluminum tri sec butoxide. Materials have been prepared without addition of citric acid in the presence of 1 (A), 2 (B) and 3 (C) g of P123.

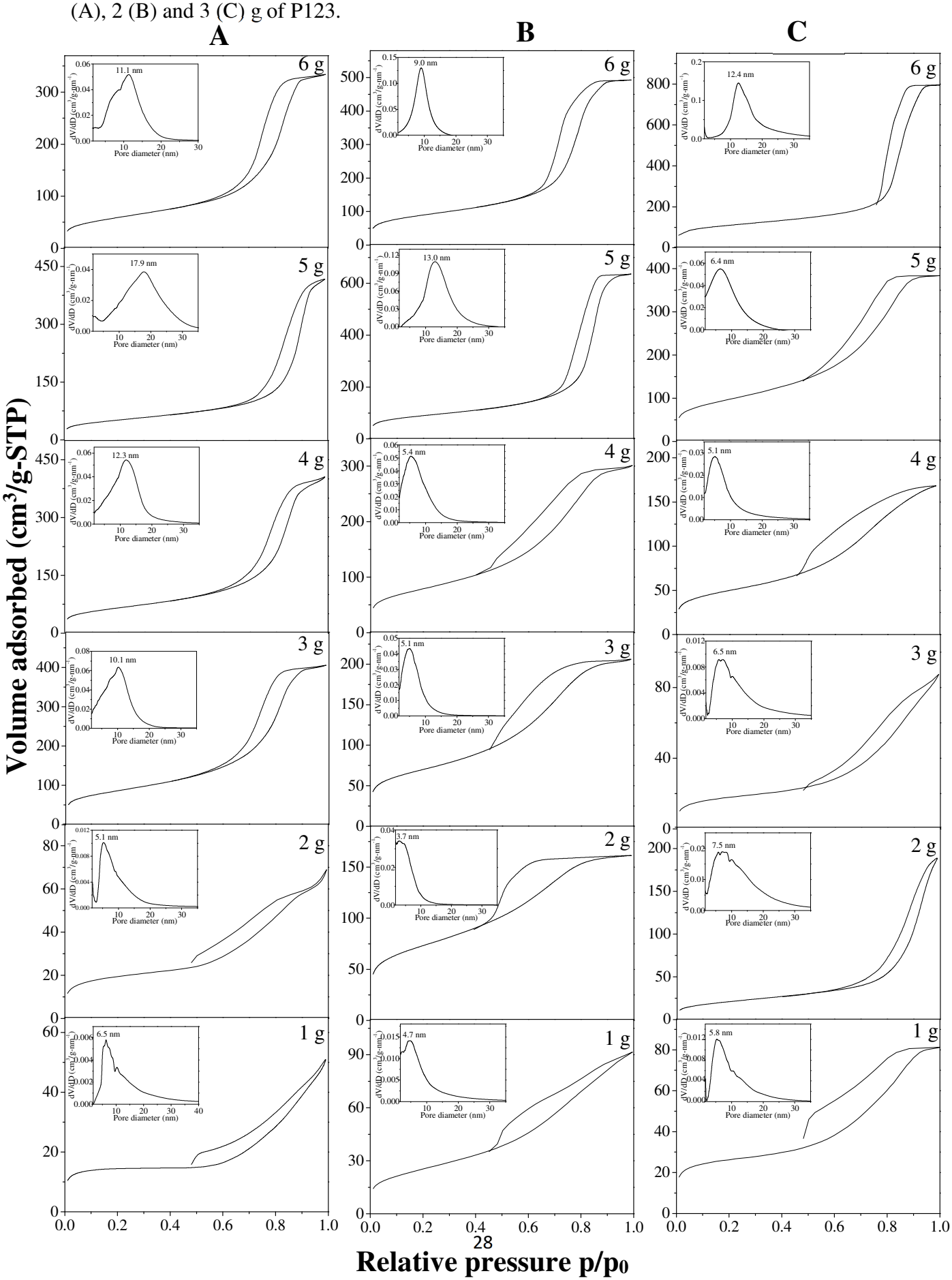

Figure S4: Variation of the SAXS patterns (a), the nitrogen adsorption-desorption isotherms (b) and the mesopores size distribution (c) as a function of the amount of both HCl (A) and citric acid (B).

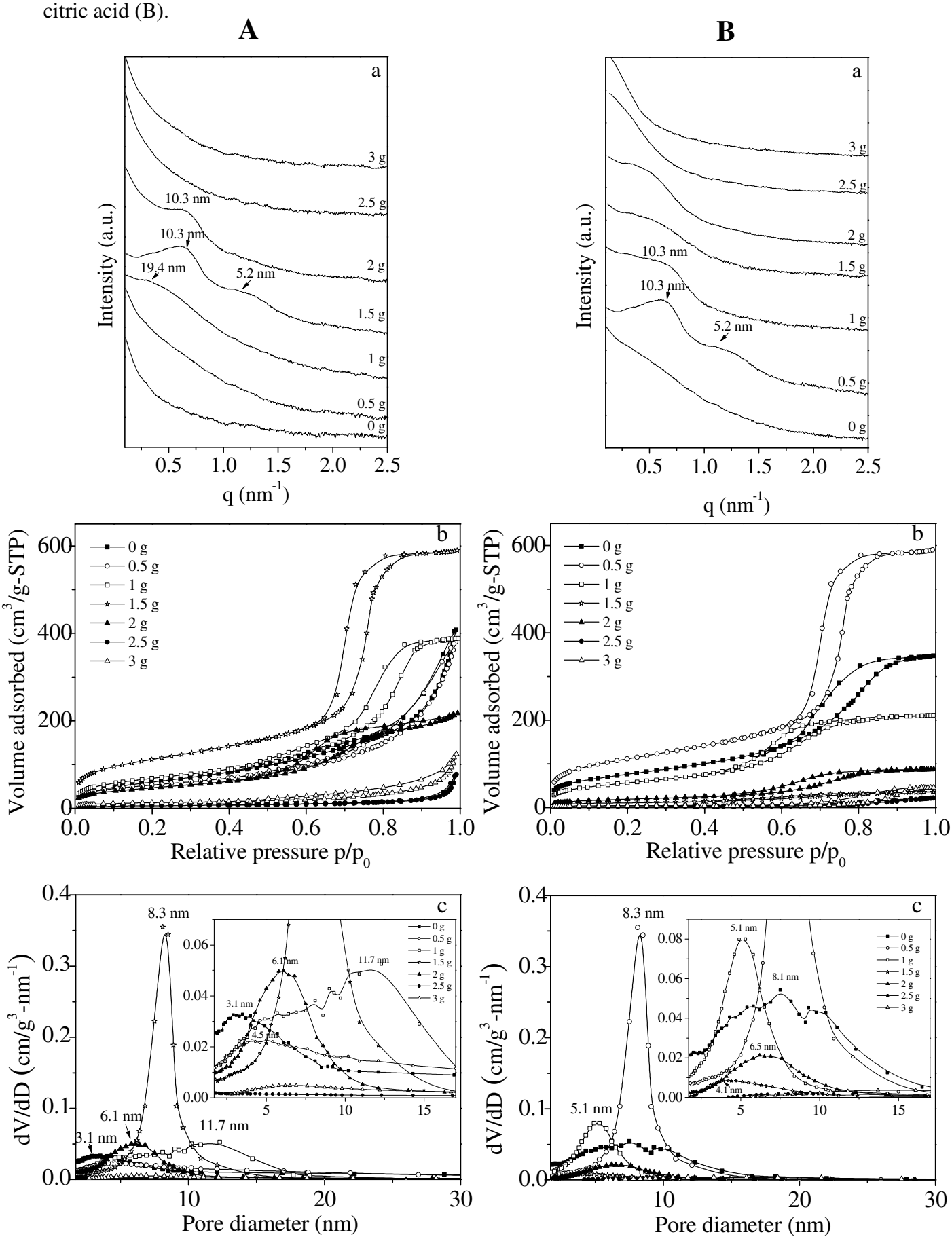

Figure S5: TEM images (A) and XRD (B) of the mesostructured alumina obtained after surfactant extraction by Soxhlet.

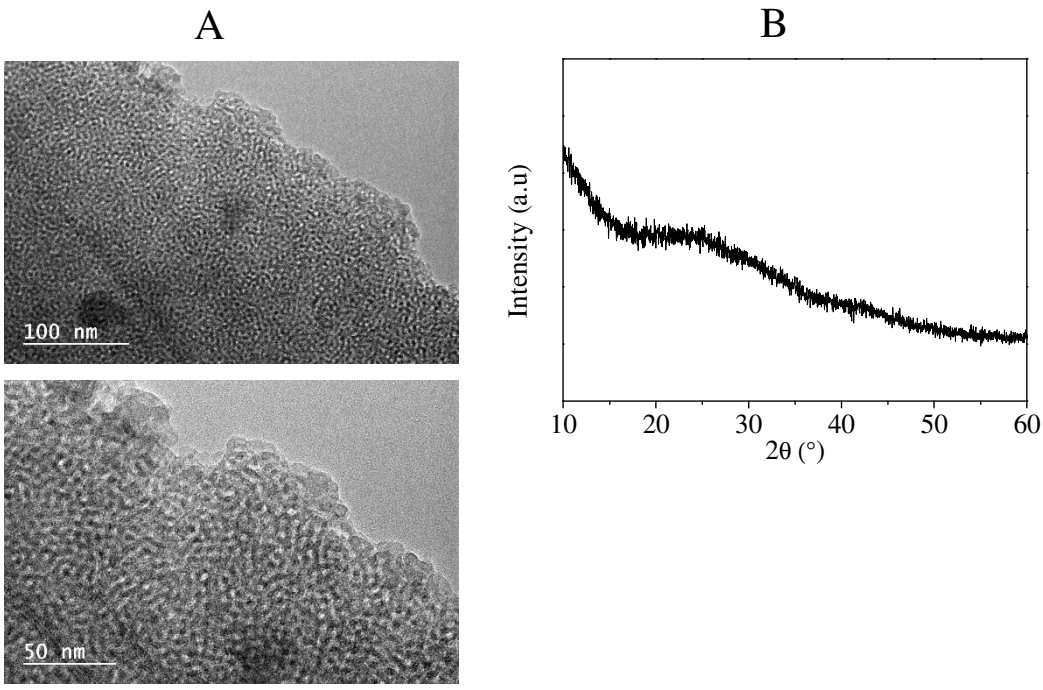

Transmission Electron Microscopy (TEM) observations were performed using a Jeol ARM-200F microscope working at 200kV.

Figure S6: EDX spectra of the as-synthesized alumina (A) and of mesostructured alumina obtained after surfactant extraction during 2 hours at room temperature by water (B) or ethanol (C).

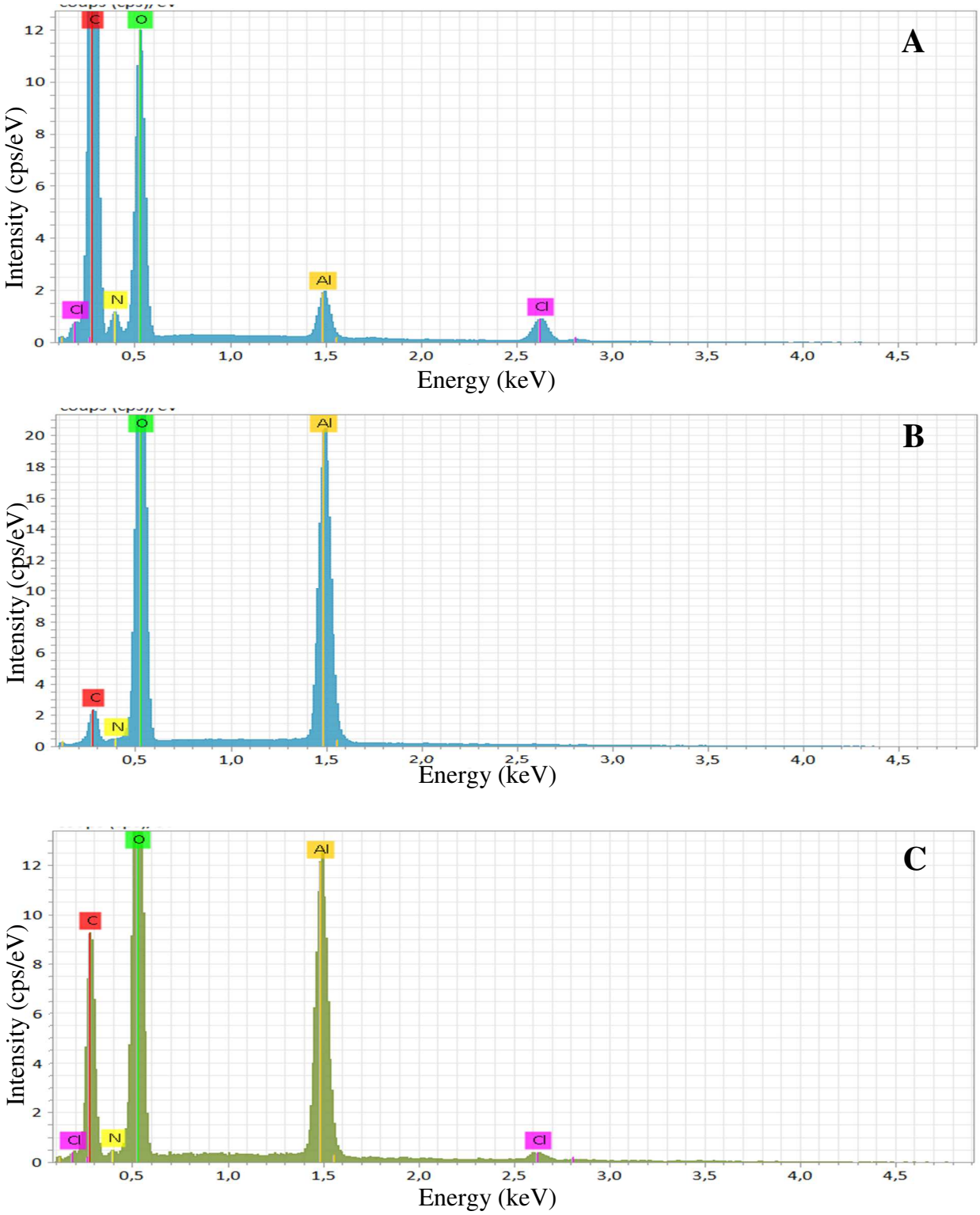

Figure S7: Evolution of the SAXS patterns as a function of the surfactant extraction by water (A) or ethanol (B) with time at room temperature.

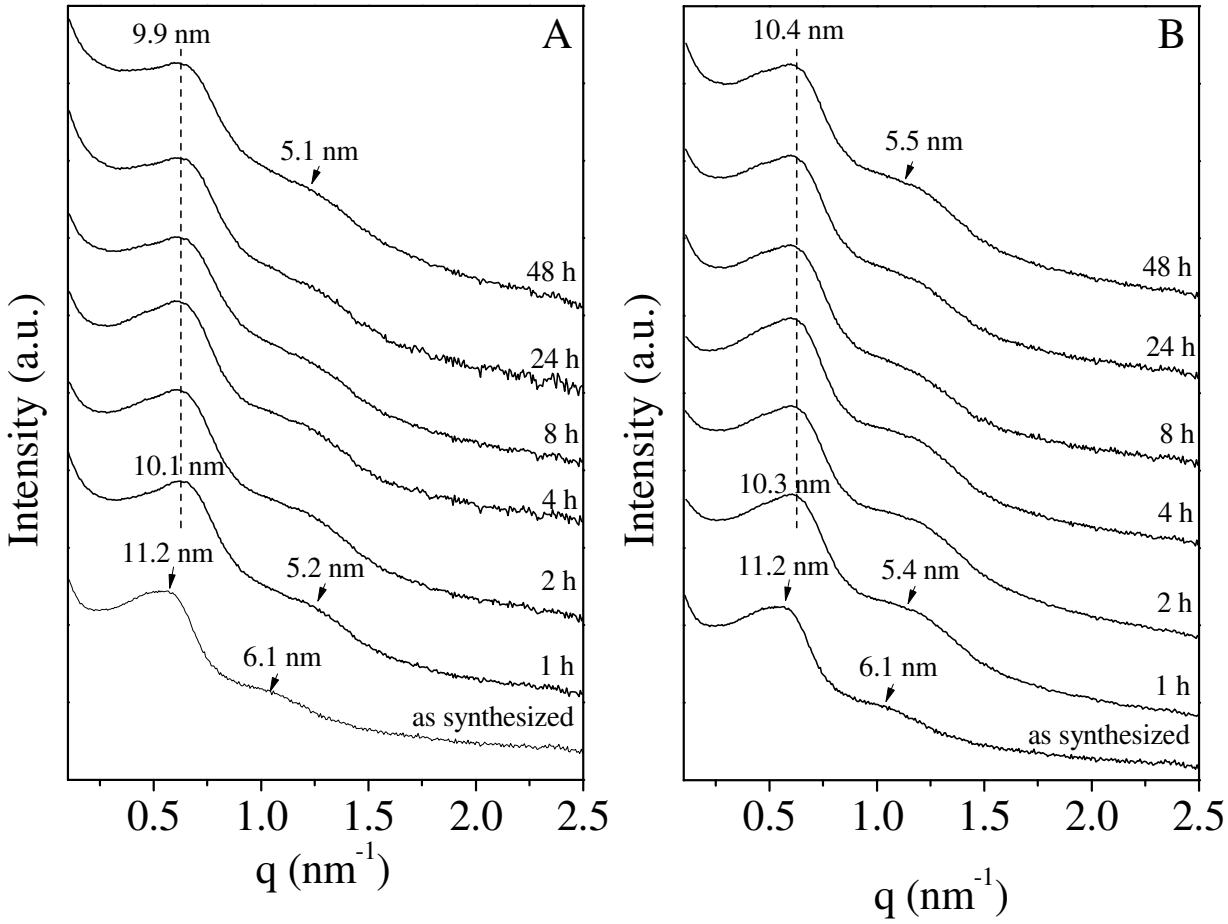

Figure S8: Variation of the nitrogen adsorption-desorption isotherms with the corresponding mesopores size distribution (insert) as a function of the surfactant extraction by water (A) or ethanol (B) with time at room temperature.

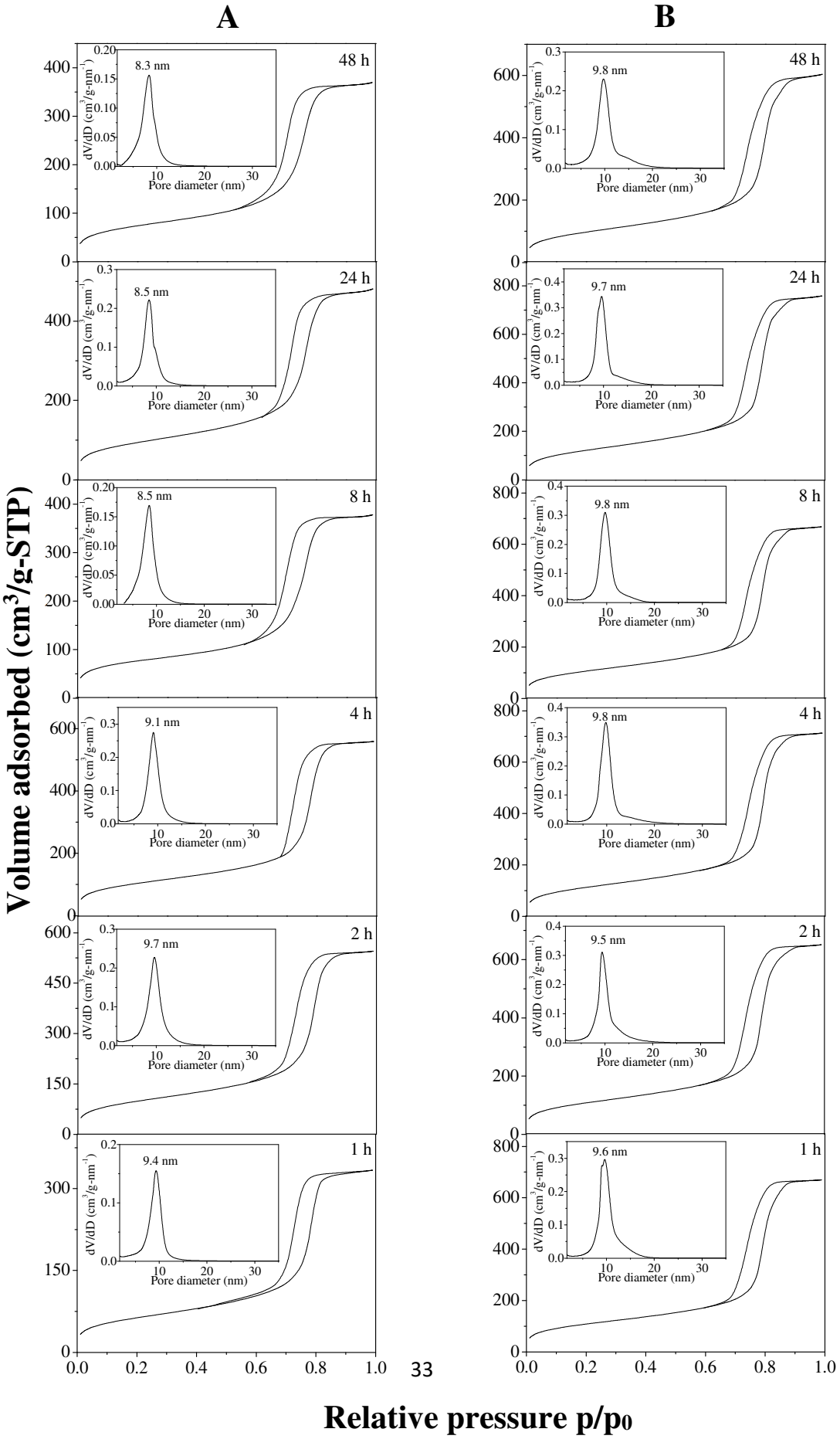

Figure S9: Evolution of the Raman spectra in the 2500-3500 cm^{-1} (a) and 700-1600 cm^{-1} (b) ranges with the extraction time by water (A) or ethanol (B) at room temperature.

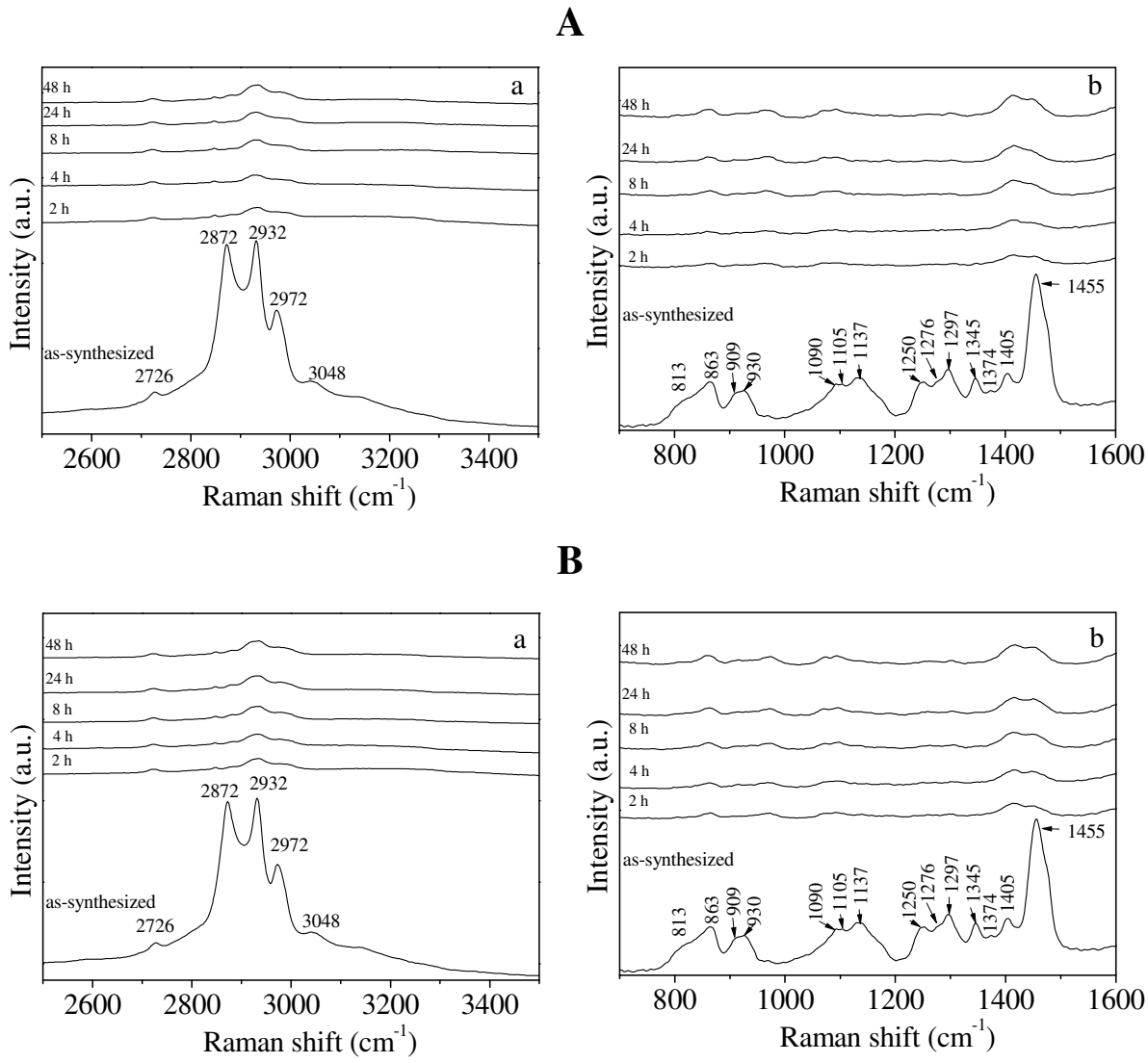

Raman Scattering Spectra were collected on a FT-Raman FRA106/S (Bruker) coupled to an Equinox IFS 55 FTIR spectrometer (Bruker). The device is equipped with a laser Nd:YAG at 1064 nm and a high sensitivity germanium detector D418. The laser power varies between 100 and 540 mW. The number of accumulations was 200 scans.

Figure S10: Evolution of the TEM images as a function of the calcination temperature.

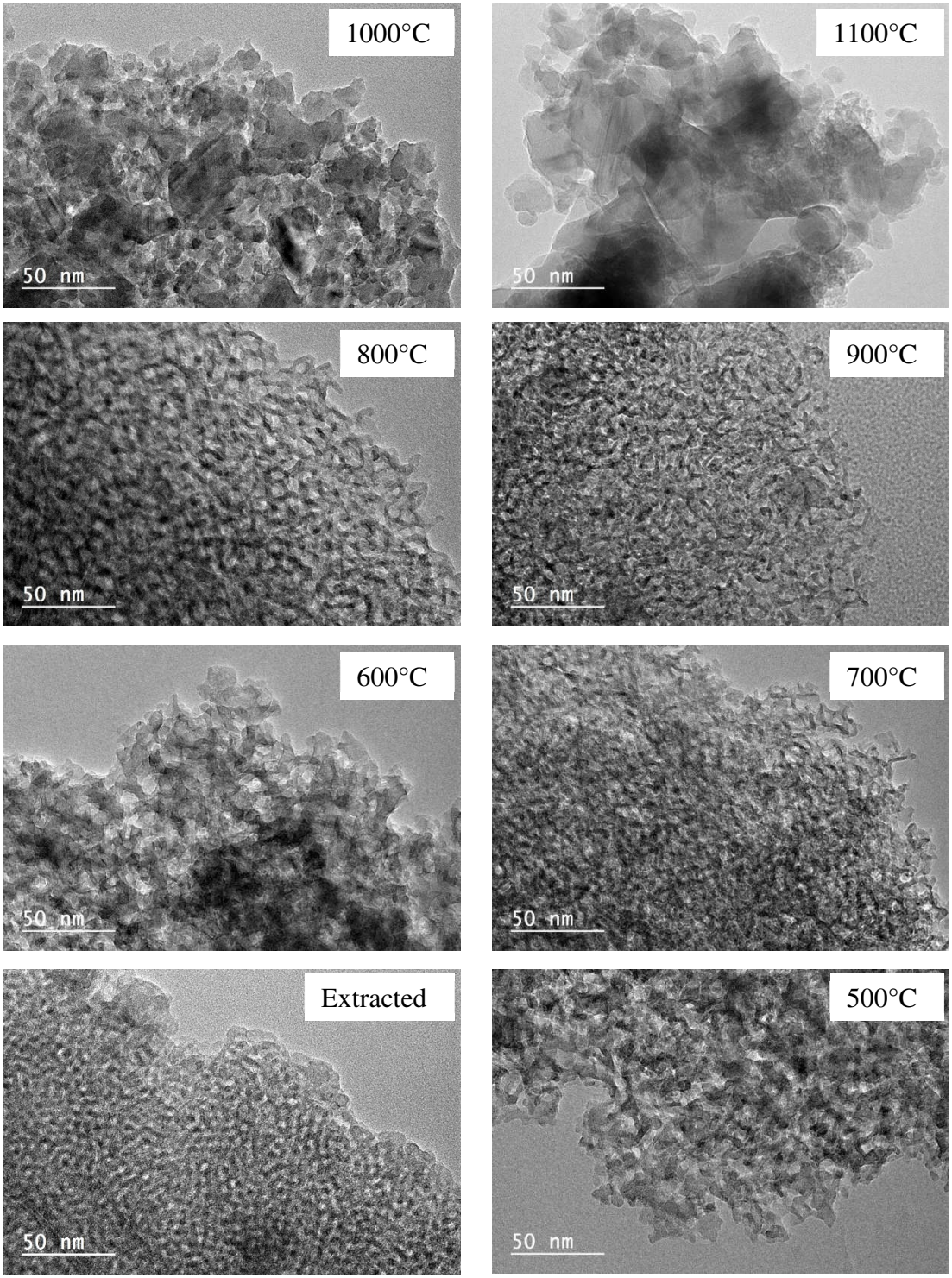

Figure S11: Evolution of SAXS pattern as a function of the immersion time in boiling water and after of exposure to water vapor. The initial mesostructured alumina has been calcined at 500°C (A), 700°C (B) or 900°C (C).